AD688168

AD

USAAVLABS TECHNICAL REPORT 69-25

APPLICATION OF MICROMECHANICS TO JOINTS AND CUTOUTS

By

Alberto Puppo

Juan Haener

April 1969

U. S. ARMY AVIATION MATERIEL LABORATORIES
FORT EUSTIS, VIRGINIA

D D C

JUN 9 1969

C

81

DISCLAIMERS

This program was carried out under Contract DAAJ02-67-C-0093 with Whittaker Corporation, Whittaker Research and Development Division, San Diego, California.

The data contained in this report are the result of an analytical and experimental study of the stress distribution in loop and bolt joints made of composite materials. Also, an analytical study was made of the stress concentration due to a circular hole in orthotropic composite sheets.

The report has been reviewed by the U.S. Army Aviation Materiel Laboratories and is considered to be technically sound. It is published for the exchange of information and the stimulation of future research.

APPLICATION OF MICROMECHANICS
TO JOINTS AND CUTOUTS

Final Report

by

Alberto Puppo
Juan Haener

Prepared by

WHITTAKER CORPORATION
Whittaker Research & Development Division
San Diego, California

for

U. S. ARMY AVIATION MATERIEL LABORATORIES
FORT EUSTIS, VIRGINIA

SUMMARY

In this report the stress distribution in loop and bolt joints made of composite materials is studied using analytical and experimental methods. Also, the stress concentration in orthotropic composite sheets with a circular hole is studied.

The numerical technique to evaluate the stresses and displacements is described. Simple design formulas to compute the stresses at critical regions are developed. A procedure of structural design is delineated and applied to specific cases.

Experimental results obtained by testing composite joints are reported. Stress distribution tests were performed using the photoelastic technique. Failure location and ultimate loads for several composite joints are shown.

This report contains the analysis of the stress concentration that appears around a circular hole in an orthotropic composite sheet under simple tension and simple shear loadings.

---

* In October 1968, Narmco Research & Development Division of Whittaker
Corporation underwent a name change to Whittaker Research & Development/
San Diego.

BLANK PAGE

TABLE OF CONTENTS

LIST OF ILLUSTRATIONS

ix

x

LIST OF TABLES

LIST OF SYMBOLS

A	total area
A_a, A_b, A_c	transverse areas of the layers a, b, c
A, B	constants
$[A]$	geometric matrix (6×6)
$[A*]$	diagonal submatrix of $[A]$, (3×3)
$[A_{ij}]$	submatrices of $[A]$
a	radius of the hole at a bolt joint
$a_1, a_2, \ldots a_6$	constants
$\{a\}$	vector of the constants $a_1, a_2, \ldots a_6$ (6×1)
b_{ij}	inverse elastic constants
$[C]$	matrix of the elements c_{ij} (3×3)
$[C_a], [C_b], [C_c]$	matrices of the elastic constants at a, b, c, referred to the axis x, y
$[C']$	matrix of the elastic constants referred to the axis x_a, y_a (x_b, y_b ; x_c, y_c , ...)
c_{ij}	elastic constants of the material
$[D]$	location matrix (3×6)
e	base of the natural logarithm
f	function of the complex variable $(Z + Y_1 \overline{Z})$
g	function of the complex variable $(Z + Y_2 \overline{Z})$
$[I]$	unit matrix
i	imaginary unit, $i = \sqrt{-1}$
$[K]$	stiffness matrix of an element (6×6)
$[K*]$	total stiffness matrix
$\left[K^*_{ij}\right]$	submatrices of $[K*]$
k^*_{ij}	element of the total stiffness matrix
ℓ, m, n	cosine directors of the directions a, b, c
P, Q	boundary load functions
$P*$	failure load
$P_{1\xi}, P_{2\xi}, \ldots P_{3\eta}$	nodal forces

xii

$\{P\}$	vector of the nodal forces (6x1)
$\{P*\}$	vector of the nodal forces for the whole structure
$\{P_1^*\}$	vector of the unknown nodal forces
$\{P_2^*\}$	vector of the known nodal forces
$\{P'\}$	vector of the rotated nodal forces
$\{P_a\},\{P_b\},\{P_c\}$	forces at the layers a,b,c
R_1,R_2	moduli of X_1,X_2
r,θ	polar coordinates
T_x	uniform tension at the x-direction
T_{xy}	shear loading
$[T]$	transformation matrix
$[T_1]$	transformation matrix of stress vector (3x3)
$[T_2]$	transformation matrix of strain vector (3x3)
t	thickness
u_r	displacement at the radial direction
u_x, u_y	displacements at the x- and y-directions, respectively
V_F	volumetric percentage of fibers in the composite
W	strain energy
X_1, X_2	auxiliary complex variables
z	complex variable
$\bar{z}$	conjugate of z
α_i	orientation angles of the nodal directions
α_1, α_2	constants dependent upon b_{ij}
$[\alpha]$	inverse matrix of $[A]$
$[\alpha_{ij}]$	submatrices of $[\alpha]$
γ_1, γ_2	constants dependent upon α_1, α_2
Δ	determinant of $[A*]$
$\{\delta\}$	displacement vector (6x1) of the nodal displacements
$\{\delta*\}$	vector of the nodal displacements for the whole structure
$\{\delta_1^*\}$	vector of the known nodal displacements

xiii

$\{\delta_2^*\}$	vector of the unknown nodal displacements
$\{\delta'\}$	vector of the rotated nodal displacements
$\epsilon_x, \epsilon_y, \gamma_{xy}$	strain components
$\epsilon_x', \epsilon_y', \gamma_{xy}'$	stresses referred to the axis x', y'
$\{\epsilon\}$	strain vector (3x1)
μ	factor of safety
ξ, η	local coordinates of the element
σ_n	normal stress component at the boundary
$\sigma_x, \sigma_y, \tau_{xy}$	stress components
$\sigma_r^*, \sigma_\theta^*$	individual failure stresses at r- and θ-directions
$\sigma_x^*, \sigma_y^*, \tau_{xy}^*$	individual failure stresses
$\sigma_x', \sigma_y', \tau_{xy}'$	stresses referred to the axis x', y'
σ	stress vector (3x1)
$\{\sigma_a\}, \{\sigma_b\}, \{\sigma_c\}$	stress vectors at the layers a,b,c
τ_{nt}	tangential stress component at the boundary
$\tau_{r\theta}$	shear stress referred to the directions r, θ
Φ	Airy function
Φ_1, Φ_2	arguments of X_1, X_2
ψ	auxiliary function
$\varphi_a, \varphi_b, \varphi_c$	orientation angles for the layers a,b,c
Ω	area of the element

The symbols (') and (") indicate first and second total differentiation, respectively.

The symbols Re[ ] and Im[ ] indicate the real and imaginary parts of the quantity within the brackets, respectively.

INTRODUCTION

In this investigat on, methods were developed for calculating and design-
ing joints of comp site materials that have directional properties. The
introduction of loads into structures, especially into thin sheets, his-
torically has presented problems, even in isotropic materials. At the
beginning of this century, such difficulties were overcome for the case
of isotropic materials. Until now, however, some simplifying assumptions
for joints of isotropic materials have been, in general, tacitly accepted.

In this work, for example, we found that the assumption of contact
stresses in the form of a cosine function in bolt joints yields unreal-
istic results, even in isotropic materials. For the present investigation,
the contact stresses were not assumed but rather were an outcome contained
in the method of solution.

First, a stiffness matrix was developed by which composites having not
only one but also n-directions of fiber layers could be taken into
account. On the basis of this development, a computer program was estab-
lished through which the stresses and displacements in a joint of arbi-
trary shape can be found. To illustrate, three sets of bolt joints
fabricated from glass fiber or boron fiber composites and an isotropic
material (e.g., steel) were calculated and studied in detail for several
bolt diameter-to-loop thickness relations. Eighteen bolt joints were
manufactured, tested, and compared with the computer results. Finally,
very simple relations for the maximum stresses were established.

A similar approach was taken to the calculation of stresses in cutouts in
composite materials. It was found that, in the contours of a circular
hole cut into a unidirectional fiber composite, the stress concentrations
are about twice that encountered in isotropic materials for certain types
of loading. For this reason, a hole in a fibrous composite must be
designed so that the fibers do not terminate in the hole but rather lead
around the hole in an uninterrupted, organic fashion. If this is done,
then cutouts in fibrous composite materials will be highly efficient com-
pared to their counterparts in isotropic materials.

Stress distributions in the fibers and in the resin matrix can be found
by using the stresses determined in this work as boundary conditions for
micromechanical analysis. Such analyses were performed under earlier Army
contracts concerned with oblique loading of a fiber reinforced com-
posite.[1,2,3]

1

METHOD FOR THE STRESS ANALYSIS OF ANISOTROPICS JOINTS OF ARBITRARY FORM

The problem is to find the stress distribution at a joint composed of an anisotropic material and of variable thickness (Figure 1).

In general, the boundary conditions are mixed; in other words, displacements or stresses are given along the boundaries.

To find the solution, we divide the joint in a certain finite number of triangles and assume that the displacements are linear functions at each one of these small triangles. Compatibility and equilibrium equations for each node of this irregular net lead us to a system of algebraic equations that permit us to obtain the displacements at each node and, with this, to determine the stress.
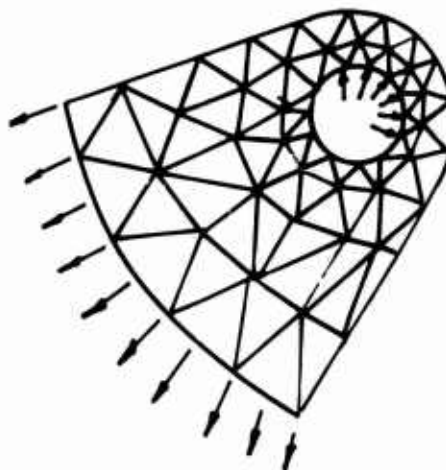
Figure 1.   Subdivision of a Joint Into Finite Elements.

Stiffness Matrix of a Triangular Element

For a triangular element (Figure 2), we assume the displacements function.[4,5,6]

$$u_x = a_1 + a_2 \xi + a_3 \eta$$

$$u_y = a_4 + a_5 \xi + a_6 \eta \tag{1}$$

where a_i are constants.

The displacements of the nodes 1, 2, and 3 are given by

$$u_{x1} = a_1$$

$$u_{x2} = a_1 + a_2 \xi_2 + a_3 \eta_2$$
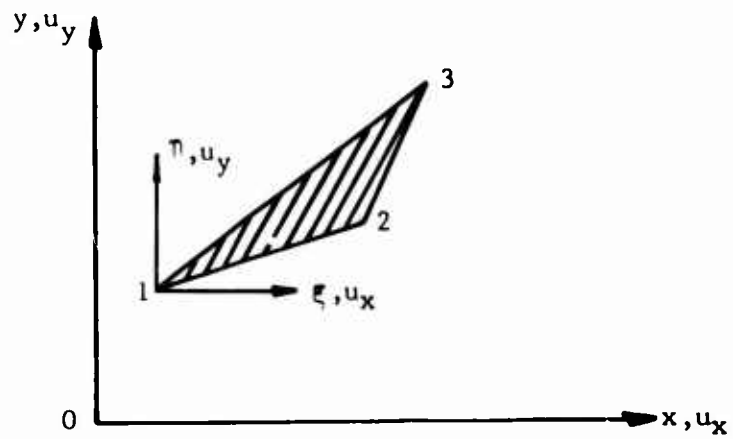
Figure 2.   Triangular Element.

$$u_{x3} = a_1 + a_2\xi_3 + a_3\eta_3$$

$$u_{y1} = a_4$$

$$u_{y2} = a_4 + a_5\xi_2 + a_6\eta_2$$

$$u_{y3} = a_4 + a_5\xi_3 + a_6\eta_3 \tag{2}$$

where ξ, η is the local coordinate system, with origin at point 1. In matrix form, the equations (2) are

$$
\begin{Bmatrix} u_{x1} \\ u_{x2} \\ u_{x3} \\ u_{y1} \\ u_{y2} \\ u_{y3} \end{Bmatrix}
=
\begin{bmatrix}
1 & 0 & 0 & 0 & 0 & 0 \\
1 & \xi_2 & \eta_2 & 0 & 0 & 0 \\
1 & \xi_3 & \eta_3 & 0 & 0 & 0 \\
0 & 0 & 0 & 1 & 0 & 0 \\
0 & 0 & 0 & 1 & \xi_2 & \eta_2 \\
0 & 0 & 0 & 1 & \xi_3 & \eta_3
\end{bmatrix}
\begin{Bmatrix} a_1 \\ a_2 \\ a_3 \\ a_4 \\ a_5 \\ a_6 \end{Bmatrix}
\tag{3}
$$

3

or

$$\{\delta\} \;=\; [A]\,\{a\} \tag{4}$$

From this equation,

$$\{a\} \;=\; [A]^{-1}\,\{\delta\} \tag{5}$$

To find the inverse of the matrix $[A]$, we write

$$[A]\,[\alpha] \;=\; [I] \qquad, \qquad [\alpha] \;=\; [A]^{-1}$$

and partition in the following manner:

$$\begin{bmatrix} [A_{11}] & [A_{12}] \\ [A_{21}] & [A_{22}] \end{bmatrix} \cdot \begin{bmatrix} [\alpha_{11}] & [\alpha_{12}] \\ [\alpha_{21}] & [\alpha_{22}] \end{bmatrix} \;=\; \begin{bmatrix} [I] & [0] \\ [0] & [I] \end{bmatrix} \tag{6}$$

Taking

$$[A_{11}] \;=\; [A_{22}] \;=\; [A*] \;=\; \begin{bmatrix} 1 & 0 & 0 \\ 1 & \xi_2 & \eta_2 \\ 1 & \xi_3 & \eta_3 \end{bmatrix} \tag{7}$$

$$[A_{21}] \;=\; [A_{12}] \;=\; [0]$$

equation (6) gives

$$[A*] \cdot [\alpha_{11}] \;=\; [A*] \cdot [\alpha_{22}] \;=\; [I]$$
$$[A*] \cdot [\alpha_{12}] \;=\; [0]$$
$$[A*] \cdot [\alpha_{21}] \;=\; [0]$$

Thus, we obtain the following:

$$[\alpha_{11}] \;=\; [\alpha_{22}] \;=\; [A*]^{-1}$$
$$[\alpha_{21}] \;=\; [\alpha_{12}] \;=\; [0] \tag{8}$$

4

Then, inverting the matrix [A*] given in equation (7), we obtain

$$[A*]^{-1} = \begin{bmatrix} \dfrac{\xi_2\eta_3 - \xi_3\eta_2}{\Delta} & 0 & 0 \\[2ex] -\dfrac{\eta_{32}}{\Delta} & \dfrac{\eta_3}{\Delta} & -\dfrac{\eta_2}{\Delta} \\[2ex] \dfrac{\xi_{32}}{\Delta} & -\dfrac{\xi_3}{\Delta} & \dfrac{\xi_2}{\Delta} \end{bmatrix} \qquad (9)$$

with
$$\Delta = \xi_2\eta_3 - \xi_3\eta_2 \qquad (10)$$

$$\xi_{ij} = \xi_i - \xi_j \quad ; \quad \eta_{ij} = \eta_i - \eta_j \quad (i,j = 1,2,3) \qquad (11)$$

Thus, the inverse of the matrix [A] is

$$[A]^{-1} = \begin{bmatrix} [A*]^{-1} & [0] \\[2ex] [0] & [A*]^{-1} \end{bmatrix} \qquad (12)$$

where $[A*]^{-1}$ is given by equation (9).

From equations (1), it is possible to obtain the strains

$$\epsilon_x = \frac{\partial u_x}{\partial \xi} = a_2$$

$$\epsilon_y = \frac{\partial u_y}{\partial \eta} = a_6$$

$$\gamma_{xy} = \frac{\partial u_x}{\partial \eta} + \frac{\partial u_y}{\partial \xi} = a_3 + a_5 \qquad (13)$$

5

or, in matrix form,

$$
\left\{ \begin{array}{c} \epsilon_x \\ \epsilon_y \\ \gamma_{xy} \end{array} \right\} = \begin{bmatrix} 0 & 1 & 0 & 0 & 0 & 0 \\ 0 & 0 & 0 & 0 & 0 & 1 \\ 0 & 0 & 1 & 0 & 1 & 0 \end{bmatrix} \cdot \left\{ \begin{array}{c} a_1 \\ a_2 \\ a_3 \\ a_4 \\ a_5 \\ a_6 \end{array} \right\}
\tag{14}
$$

Symbolically, we write equation (14) in the form

$$
\{\epsilon\} = [D] \cdot \{a\}
\tag{15}
$$

Substituting $\{a\}$ given by equation (5) into the last equation, we obtain

$$
\{\epsilon\} = [D] \cdot [A]^{-1}\{\delta\}
\tag{16}
$$

On the other hand, the relationship between stresses and strains for an anisotropic material and the two-dimensional problem is

$$
\left\{ \begin{array}{c} \sigma_x \\ \sigma_y \\ \tau_{xy} \end{array} \right\} = \begin{bmatrix} c_{11} & c_{12} & c_{13} \\ c_{12} & c_{22} & c_{23} \\ c_{13} & c_{23} & c_{33} \end{bmatrix} \left\{ \begin{array}{c} \epsilon_x \\ \epsilon_y \\ \gamma_{xy} \end{array} \right\}
\tag{17}
$$

or

$$
\{\sigma\} = [C]\{\epsilon\}
\tag{18}
$$

Putting equation (16) into equation (18), we get

$$
\{\sigma\} = [C][D][A]^{-1}\{\delta\}
\tag{19}
$$

6

The strain energy is given by

$$W = \frac{1}{2} \int_V \left(\epsilon_x \sigma_x + \epsilon_y \sigma_y + \gamma_{xy} \tau_{xy} \right) \, dV$$

$$= \frac{1}{2} \int \int t \left[\epsilon_x \ \epsilon_y \ \gamma_{xy} \right] \cdot \begin{Bmatrix} \sigma_x \\ \sigma_y \\ \tau_{xy} \end{Bmatrix} dx \ dy = \frac{1}{2} \int \int t \ \{\epsilon\}^T \cdot \{\sigma\} \ dx \ dy \tag{20}$$

where t is the thickness of the joint and $\{\epsilon\}^T$ is the transposed vector of $\{\epsilon\}$. But

$$\{\epsilon\}^T = \left([D] \cdot \{a\} \right)^T = \{a\}^T \, [D]^T$$

$$= \left([A]^{-1} \cdot \{\delta\} \right)^T [D]^T = \{\delta\}^T \left([A]^{-1} \right)^T [D]^T \tag{21}$$

where we used equations (15) and (5). With equations (19) and (21), the strain energy is expressed by

$$W = \frac{1}{2} \int \int t \ \{\delta\}^T \left([A]^{-1} \right)^T [D]^T [C] [D] [A]^{-1} \{\delta\} \ dx \ dy \tag{22}$$

Now we can assume that the forces $P_{1\xi}$, $P_{2\xi}$, $P_{3\xi}$, $P_{1\eta}$, $P_{2\eta}$, and $P_{3\eta}$ are applied on the triangle vertex, as shown in Figure 3.
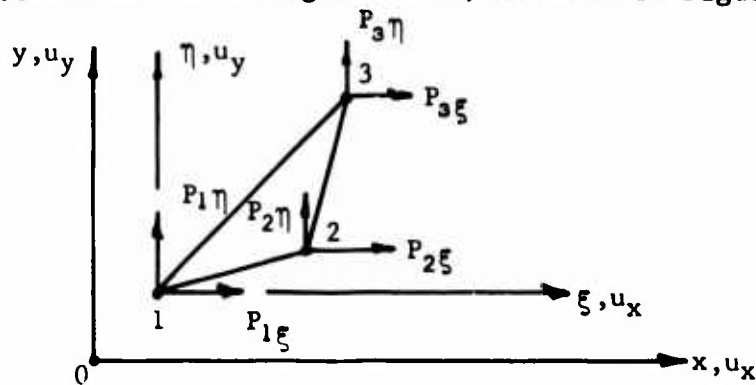
Figure 3. Generalized Nodal Forces.

7

We can define a stiffness coefficient k^*_{ij} as the force that is necessary to apply at i direction when the displacement at j direction is the unit and all other displacements are zero. The directions i and j can be any one of $P_{1\xi}$, $P_{2\xi}$, ... $P_{3\eta}$. If, for example, $u_{x2} = 1$ and $u_{x1} = u_{x3} = u_{y1} = u_{y2} = u_{y3} = 0$, the stiffness coefficients k_{i2} are the forces that we need to apply at directions of $P_{1\xi}$, $P_{2\xi}$, ... $P_{3\eta}$, to keep this deformation of the triangle.

To compute the stiffness coefficients, we will use the second Castigliano theorem, which permits us to find the generalized force by differentiation of the total strain energy with respect to the corresponding displacement. Thus,

$$P_i = \frac{\partial W}{\partial \delta_i} \tag{23}$$

Then, by differentiation of equation (22) with respect to $\{\delta\}$, we have

$$\{P\} = \int \int t \left([A]^{-1}\right)^T [D]^T [C] [D] [A]^{-1} \, dx \, dy \cdot \{\delta\} \tag{24}$$

and the stiffness matrix $[K]$ yields

$$[K] = \int \int t \left([A]^{-1}\right)^T [D]^T [C] [D] [A]^{-1} \, dx \, dy \tag{25}$$

Assuming that the thickness of the triangle is constant, the stiffness matrix becomes

$$[K] = \left([A]^{-1}\right)^T [D]^T [C] [D] [A]^{-1} \cdot t \, \Omega \tag{26}$$

with Ω equal to the area of the triangle.

Equation (24) can be written as

$$\{P\} = [K] \{\delta\} \tag{27}$$

which is referred to the axis x,y or, in other words, ξ,η . However, for certain special mixed boundary conditions, it would be useful to

8

refer equation (27) to the rotated axis. The rotations are α_1, α_2, and α_3 at the nodes 1, 2, and 3, respectively, as shown in Figure 4.
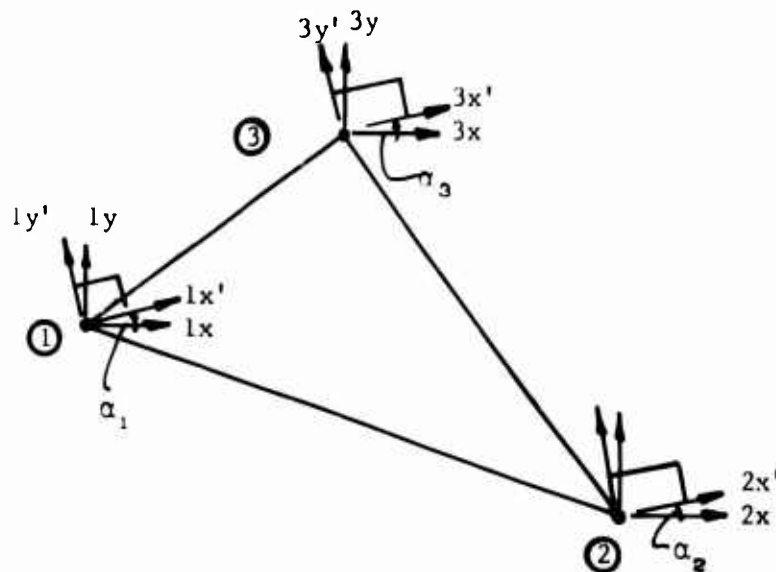
Figure 4. Rotation of the Nodal Directions.

The rotated forces vector $\{P'\}$ is related to $\{P\}$ as

$$
\begin{Bmatrix} P_{1x} \\ P_{2x} \\ P_{3x} \\ P_{1y} \\ P_{2y} \\ P_{3y} \end{Bmatrix} = \begin{bmatrix} \cos\alpha_1 & 0 & 0 & -\sin\alpha_1 & 0 & 0 \\ 0 & \cos\alpha_2 & 0 & 0 & -\sin\alpha_2 & 0 \\ 0 & 0 & \cos\alpha_3 & 0 & 0 & -\sin\alpha_3 \\ \sin\alpha_1 & 0 & 0 & \cos\alpha_1 & 0 & 0 \\ 0 & \sin\alpha_2 & 0 & 0 & \cos\alpha_2 & 0 \\ 0 & 0 & \sin\alpha_3 & 0 & 0 & \cos\alpha_3 \end{bmatrix} \begin{Bmatrix} P'_{1x} \\ P'_{2x} \\ P'_{3x} \\ P'_{1y} \\ P'_{2y} \\ P'_{3y} \end{Bmatrix}
$$

(28)

or, in condensed form,

$$\{P\} = [T]\{P'\} \tag{29}$$

9

Analogously, we can write

$$\{\xi\} = [T] \{\xi'\} \tag{30}$$

By substituting equations (29) and (30) into equation (27), we obtain

$$\{P'\} = [K'] \{\delta'\} \tag{31}$$

where $[K']$ is the rotated stiffness matrix given by

$$[K'] = [T]^{-1} [K] [T] \tag{32}$$

The total stiffness matrix of the whole structure can be obtained by summing in adequate order the elements of the matrices $[K']$ of each element. The law of formation for the elements of the total stiffness matrix $[K*]$ is

$$k^*_{ij} = \sum_{n=1}^{N} k'^{n}_{ij} \tag{33}$$

where k^*_{ij} is an element of $[K*]$ and k'^{n}_{ij} is the element of the matrix $[K']$ for the triangle n after the conversion of indices i, j from the indices 1 through 6 to the actual indices of the whole structure. The summation is extended to the N triangles.

If the numbering of the nodal directions is started by the directions in which the displacement is known, the matrix equilibrium equation for the whole structure

$$[K*] \{\delta*\} = \{P*\} \tag{34}$$

can be partitioned as

$$\begin{bmatrix} [K^*_{11}] & [K^*_{12}] \\ [K^*_{21}] & [K^*_{22}] \end{bmatrix} \begin{Bmatrix} \{\delta^*_1\} \\ \{\delta^*_2\} \end{Bmatrix} = \begin{Bmatrix} \{P^*_1\} \\ \{P^*_2\} \end{Bmatrix} \tag{35}$$

10

where $\{\delta_1^*\}$ is the vector of the known nodal displacements

$\{\delta_2^*\}$ is the vector of the unknown nodal displacements

$\{P_1^*\}$ is the vector of the unknown nodal forces

$\{P_2^*\}$ is the vector of the known nodal forces

The second row of equation (35) can be written as

$$[K_{22}^*] \{\delta_2^*\} = \{P_2^*\} - [K_{21}^*] \{\delta_1^*\} \qquad (36)$$

This is a system of linear equations that, when solved, enables us to know the displacements $\{\delta_2^*\}$. Once that $\{\delta_2^*\}$ is known, the first row of equation (35) gives the nodal forces $\{P_1^*\}$.

When all the nodal displacements are known, the stresses can be determined by substituting the displacements $\{\delta\}$, corresponding to each triangle, in equation (19).

It must be noted that the stresses become constant at each triangle. Thus, to have a good approximation, the triangular net must be more dense in those places where the stress gradient is greater, as occurs in areas of stress concentrations.

The stress diagrams can be smoothed out adequately by taking the average of stresses between two adjacent triangles and assigning this average to the midpoint of the common side.

Computation of the Matrix [C] Elements

In the most general case we can assume that the material contains, at an arbitrary point, fibers in n-directions. For the following development, we take only three different directions, a, b, and c, but the generalization to any number of directions is immediate.

We refer the material to the axes x and y (Figure 5). If we impose a deformation $\{\epsilon\}$, the materials with fibers at directions a, b, and c each have the stresses
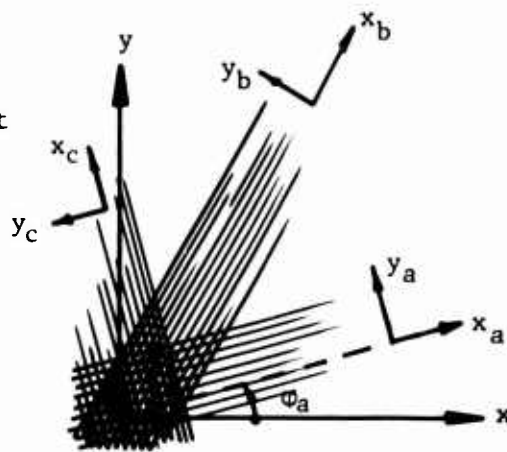

Figure 5. Multilayered Composite.

$$\{\sigma_a\} = [C_a]\{\epsilon\} \quad , \quad \{\sigma_b\} = [C_b]\{\epsilon\} \quad , \quad \{\sigma_c\} = [C_c]\{\epsilon\} \qquad (37)$$

11

where the vectors $\{\sigma_a\}$, $\{\sigma_b\}$, and $\{\sigma_c\}$ and the matrices $[C_a]$, $[C_b]$, and $[C_c]$ are referring to axes x and y.

Considering a certain total area A composed of the areas A_a, A_b, and A_c corresponding to the three materials, that is to say,

$$A = A_a + A_b + A_c \tag{38}$$

the forces produced by the imposed deformation are

$$\{P_a\} = A_a \{\sigma_a\} = A_a [C_a] \{\epsilon\}$$
$$\{P_b\} = A_b \{\sigma_b\} = A_b [C_b] \{\epsilon\}$$
$$\{P_c\} = A_c \{\sigma_c\} = A_c [C_c] \{\epsilon\} \tag{39}$$

Then the total force is

$$\{P\} = \{P_a\} + \{P_b\} + \{P_c\}$$

or, by using equations (39),

$$\{P\} = \left(A_a [C_a] + A_b [C_b] + A_c [C_c] \right) \{\epsilon\} \tag{40}$$

On the other hand, it is possible to assume that $\{P\}$ is produced by a stress $\{\sigma\}$ applied on the total area A ,

$$\{P\} = A \{\sigma\} \tag{41}$$

Comparing equations (40) and (41), we find

$$\{\sigma\} = \left(\frac{A_a}{A} [C_a] + \frac{A_b}{A} [C_b] + \frac{A_c}{A} [C_c] \right) \{\epsilon\} \tag{42}$$

Thus we arrive at a matrix $[C]$ given by

$$[C] = n_a [C_a] + n_b [C_b] + n_c [C_c] \tag{43}$$

12

where $\quad n_a = \dfrac{A_a}{A} \quad , \quad n_b = \dfrac{A_b}{A} \quad , \quad n_a + n_b + n_c = 1 \qquad (44)$

If the matrix material (resin) is the same for the three materials, which is the most common case, the numbers n_a , n_b , and n_c are proportional to the number of fibers (or layers) at each direction a , b , or c.

Referring the elastic constants for the material $\underline{a}$ to the axis x_a , y_a (Figure 5), we have[7]

$$\begin{Bmatrix} \sigma'_x \\ \sigma'_y \\ \tau'_{xy} \end{Bmatrix} = \begin{bmatrix} c'_{11} & c'_{12} & 0 \\ c'_{12} & c'_{22} & 0 \\ 0 & 0 & c'_{33} \end{bmatrix} \begin{Bmatrix} \varepsilon'_x \\ \varepsilon'_y \\ \gamma'_{xy} \end{Bmatrix} \qquad (45)$$

because x_a , y_a are principal axes of orthotropy for the material $\underline{a}$. Equation (45) can be written in briefer form, as follows:

$$\{\sigma'_a\} = [C'_a] \{\varepsilon'_a\} \qquad (46)$$

Now we want to transfer equation (46) from axis x_a, y_a to axis x, y . The stresses are transformed by the following equation:

$$\{\sigma'_a\} = [T_{1a}] \{\sigma_a\} \qquad (47)$$

where

$$[T_{1a}] = \begin{bmatrix} \ell_a^2 & m_a^2 & 2\ell_a m_a \\ m_a^2 & \ell_a^2 & -2\ell_a m_a \\ -\ell_a m_a & \ell_a m_a & \ell_a^2 - m_a^2 \end{bmatrix} \qquad (48)$$

and

$$\ell_a = \cos \varphi_a \quad , \quad m_a = \sin \varphi_a \qquad (49)$$

The strains are transformed by

$$\{\varepsilon'_a\} = [T_{2a}] \{\varepsilon_a\} \qquad (50)$$

13

with

$$[T_{2a}] = \begin{bmatrix} \ell_a^2 & m_a^2 & \ell_a m_a \\ m_a^2 & \ell_a^2 & -\ell_a m_a \\ -2\ell_a m_a & 2\ell_a m_a & \ell_a^2 - m_a^2 \end{bmatrix} \tag{51}$$

Substituting equations (47) and (50) into equation (46) and then multiplying both members by $[T_{1a}]^{-1}$ gives us

$$\{\sigma_a\} = [T_{1a}]^{-1} [C_a'] [T_2] \{\varepsilon\} \tag{52}$$

Thus, by comparison of equations (52) and the first equation (37), we find

$$[C_a] = [T_{1a}]^{-1} [C_a'] [T_{2a}] \tag{53}$$

In the same way, it is possible to find matrices $[C_b]$ and $[C_c]$, using the transformation matrix $[T_{1b}]$, $[T_{1c}]$, $[T_{2b}]$, and $[T_{2c}]$.

Thus, the following steps are necessary to find matrix $[C]$ of a triangle:

1. Establish angle orientations φ_a, φ_b, and φ_c of the fibers.
2. Establish the fiber proportions at each direction n_a, n_b, and n_c.
3. On the base of the constants for each layer, obtain $[C_a]$, $[C_b]$, and $[C_c]$ by using equation (53).
4. By applying equation (43), compute $[C]$.

The elastic constants for each layer can be obtained with the formulas for unidirectional composites based on the fiber volumetric content and the elastic properties of the fiber and matrix material.

Computer Program

With the elements developed in this section, a computer program was devised which enabled us to establish the stresses and displacements for a joint. The shape of the joint can be arbitrary as well as the system of applied loads. In other words, the joint can be solved under arbitrary mixed boundary conditions. This program also covered a very

14

specific boundary condition that appears when the displacement component at the normal direction of a curved boundary is restricted and also when nonfriction is prescribed.

The thickness of the joint can be variable. The analysis can be performed for any anisotropic material with variable elastic properties.

STRESS ANALYSIS OF BOLT JOINTS

Basic Assumptions

The stress analysis performed during this contract was concerned primarily with finding the stresses in a bolt joint under tension (Figure 6).
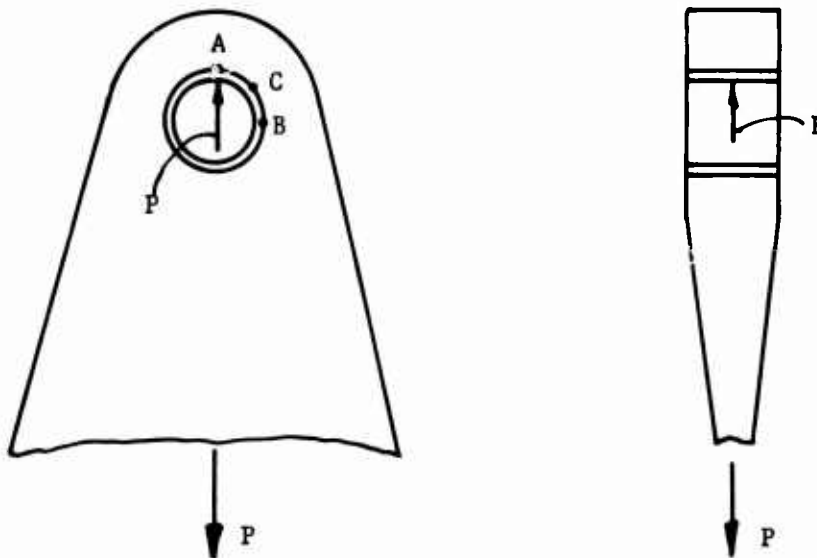

Figure 6. Typical Joint.

Between the bolt and the joint there is a bushing of bronze or steel which prevents the composite material from coming into direct contact with the steel bolt.

Critical points in a stress analysis of this type of joint are the boundary conditions to be taken along the hole contour in contact with the bushing. Many investigators adopted the cosine law for the pressure distribution on the bolt.[8] However, the stress distribution obtained on the

15

basis of this assumption does not correlate with the experimental results, especially in the prediction of the point of initial failure. In fact, if the hypothesis of the cosine law pressure distribution is adopted, the critical point is A in Figure 6 while the actual point is indicated at a position such as C. A more realistic stress distribution is obtained by assuming that the radial displacement on the boundary ACB is zero, and that there is no friction between bolt and joint. The pressure distribution on the hole boundary obtained from this hypothesis shows a considerable difference with respect to the cosine distribution. Thus, the boundary conditions adopted in the following analysis are those depicted in Figure 7.

1. On the external boundary:

$$\sigma_n = \tau_{nt} = 0$$

where n,t indicates the normal and tangential directions, respectively.

2. On the hole boundary ACB:

$$u_r = 0$$

$$\tau_{r\theta} = 0$$

with r and θ, polar coordinates, as indicated in Figure 7.

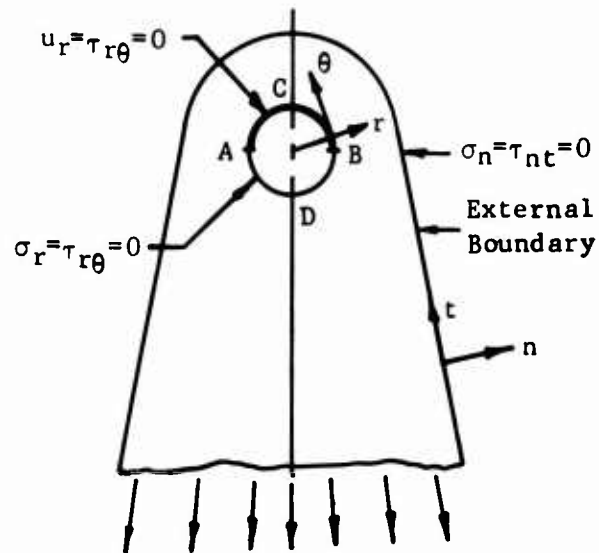3. On the hole boundary ADB:

$$\sigma_r = \tau_{r\theta} = 0$$

Figure 7. Boundary Conditions.

These boundary conditions correspond to a tension loading on the joint.

Stress Distributions

The stress distribution of joints was established by using the computer program developed on the basis of the elements given in the preceding section. A parametric study was conducted to find the differences between the stress distribution obtained in an isotropic joint and those in fiber reinforced joints, both with the same geometric characteristics.

16

A joint was selected with a ratio
$t/a = 1.02$ (see Figure 8), which is
used frequently in the applications.
The following figures show the radial
and tangential stresses σ_r and σ_θ
in the joint for different materials.
The stresses σ_r are all compression
and σ_θ are all tension. The shear
stress $\tau_{r\theta}$ can be considered
zero for practical purposes. Thus,
the stress trajectories of tension
are approximately concentric circles,
and the compression trajectories are
radial straight lines. The stress
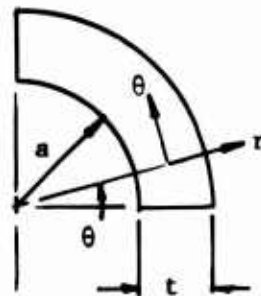diagrams shown in the figures corres-
pond to the following cases:

Figure 8.   Dimensions and
Coordinate Axis.

Figure No.	Material
9	Isotropic (steel)
10	Unidirectional glass composite with $V_F = 0.6$
11	Unidirectional glass composite with $V_F = 0.7$
12	Unidirectional glass composite with $V_F = 0.8$
13	Unidirectional boron composite with $V_F = 0.7$

The term unidirectional composite indicates that all the fibers in the
part being studied (Figure 8) are parallel to the circular boundaries.
V_F indicates the volume content of fibers.

The stresses plotted in Figures 9 through 13 correspond to a total applied
tension force $P = 2t$; in other words, the average stress $(\sigma_\theta)_{\theta=0}$ is
unity. From the analysis of these stress diagrams, it is possible to
draw the following conclusions:

1. The peaks of both stresses σ_r and σ_θ are on the
    internal boundary.

2. The maximum difference between the peak values of
    σ_r is less than 15% (from 1.14 to 1.32).

3. The difference in the stresses σ_θ on the boundary
    in the critical area $20° < \theta < 80°$ is less than 10%.

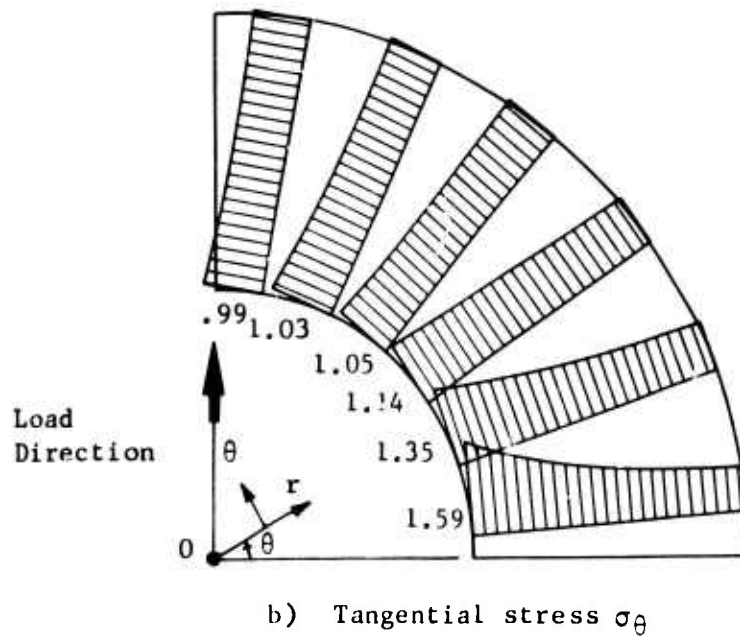4. The shapes of the stress diagrams are essentially
    the same.

17

a) Radial stress σ_r
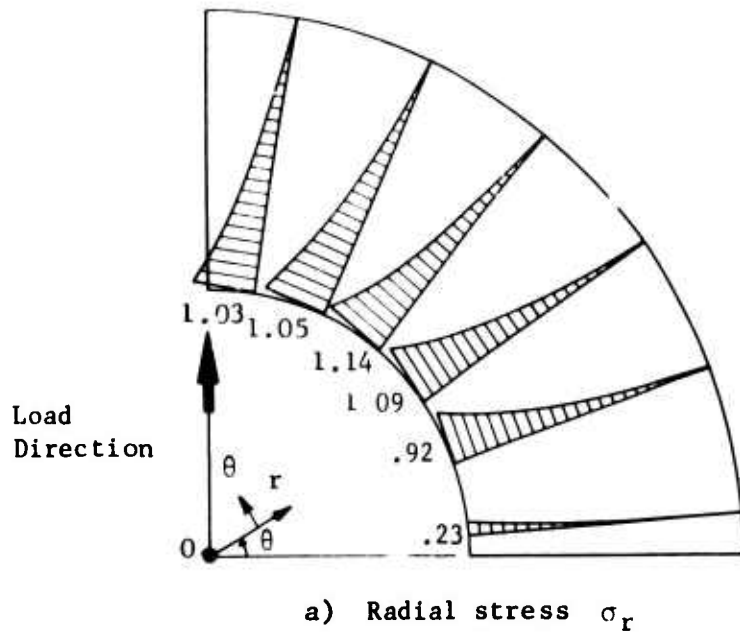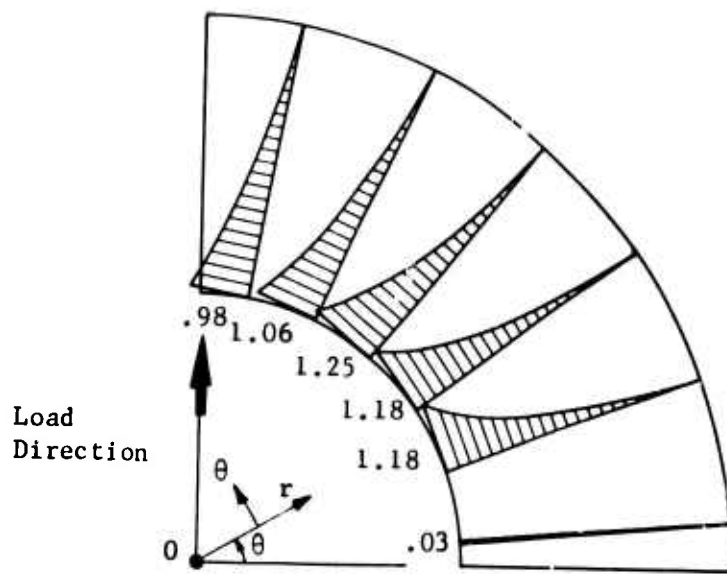

b) Tangential stress σ_θ

Figure 9. Stress Diagrams for Isotropic Material (Steel).

18

a) Radial stress σ_r
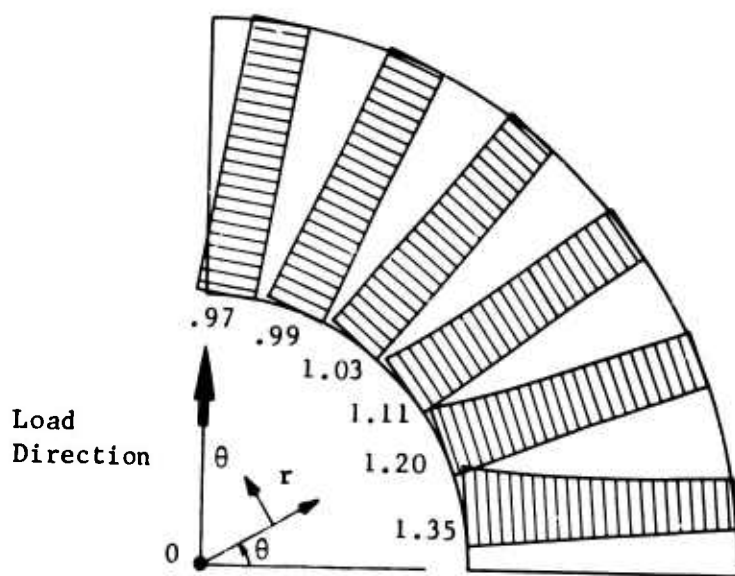
b) Tangential stress σ_θ

Figure 10. Stress Diagrams for Glass Composite Material ($V_F = 0.6$).
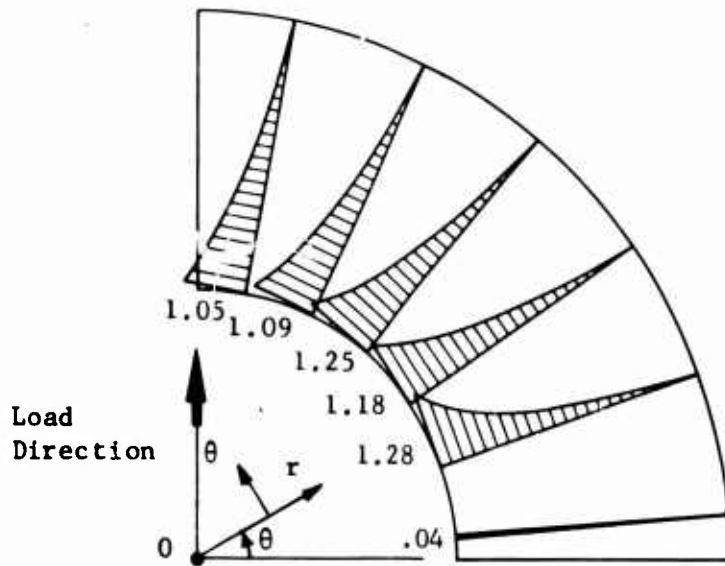
a) Radial stress σ_r
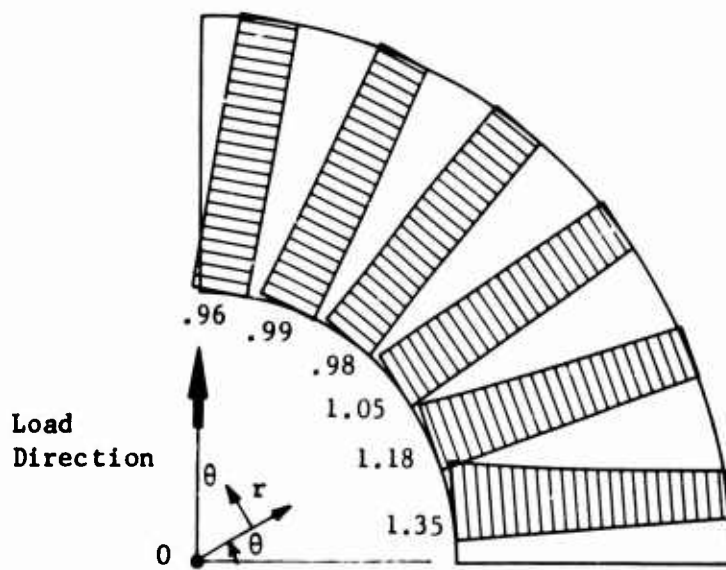
b) Tangential stress σ_θ

Figure 11. Stress Diagrams for Glass Composite Material (V_F = 0.7).
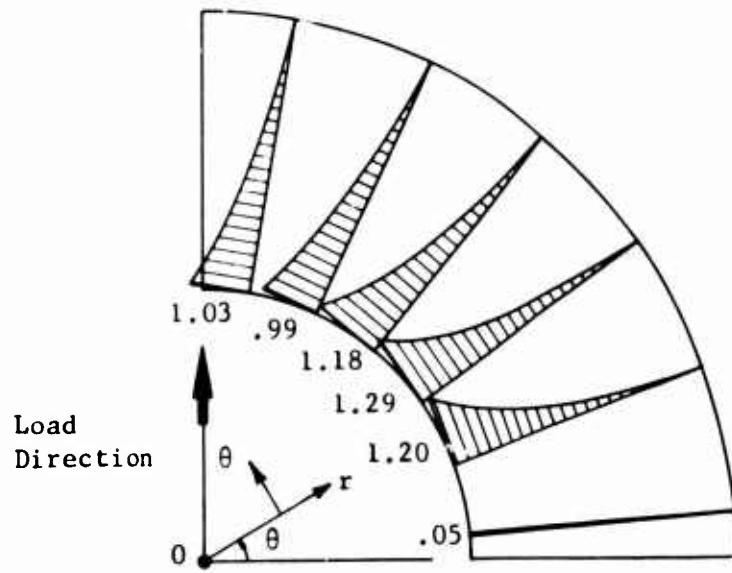
a) Radial stress σ_r
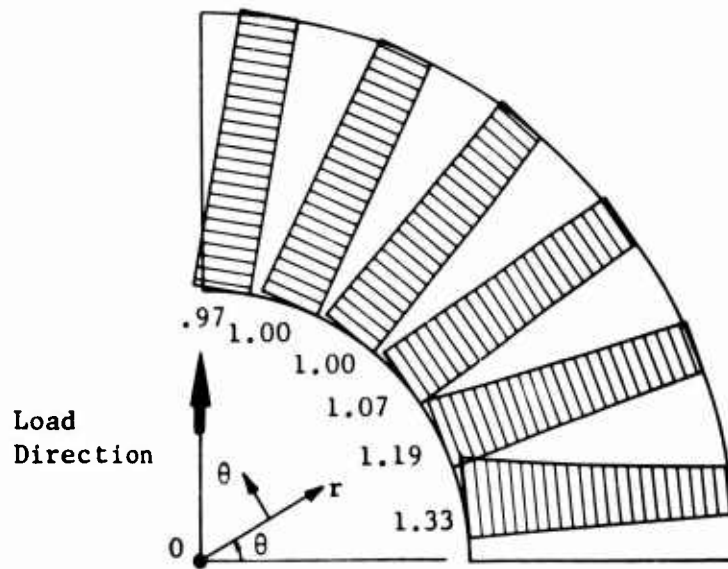
b) Tangential stress σ_θ

Figure 12. Stress Diagrams for Glass Composite Material ($V_F = 0.8$).

21

a) Radial stress σ_r

b) Tangential stress σ_θ
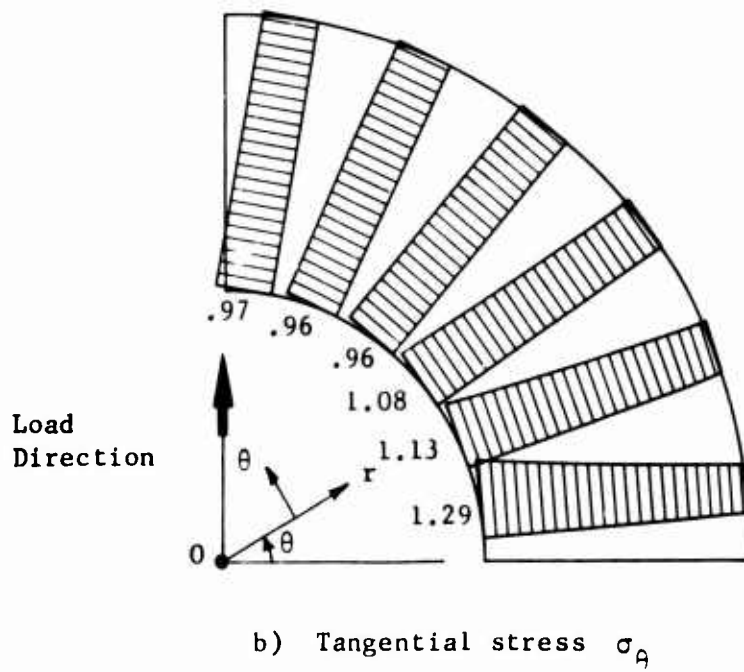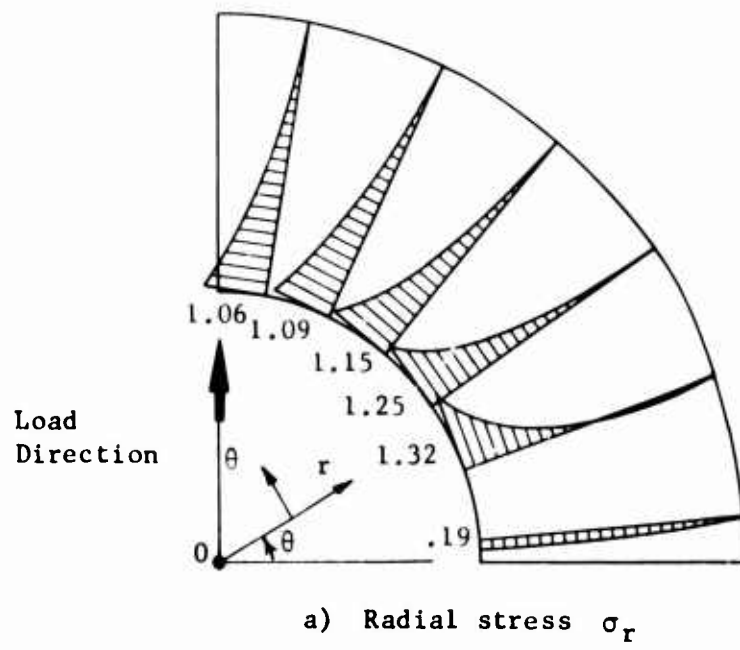
Figure 13. Stress Diagrams for Boron Composite Material ($V_F = 0.7$).

22

It is therefore possible to analyze the stresses in this type of joint by assuming the isotropy of the material. The resultant stresses will, for design purposes, be sufficiently accurate.

Another type of parametric study was performed in order to establish the variation of the stresses with respect to the changes of the ratio t/z. Two types of materials, isotropic and glass composite $(V_F = 0.7)$, were also considered. Table I gives the characteristics of the joints for which stresses are shown in Figures 14 through 19.

TABLE I. CHARACTERISTICS OF JOINTS				
Figure No.	Material	Ratio $\frac{t}{a}$	Maximum, σ_r	σ_θ where σ_r is maximum
14	Isotropic	0.57	0.68	1.07
15	Glass composite	0.57	0.59	0.98
16	Isotropic	1.14	1.28	1.08
17	Glass composite	1.14	1.22	1.02
18	Isotropic	1.71	2.00	1.29
19	Glass composite	1.71	1.92	1.20

The results shown in this table confirm the conclusion of the preceding parametric study referring to the small influence of the material properties on the maximum stresses.

23

Load
Direction

θ

r

θ

0

.58
.62
.64
.68
.62
.08

a)   Radial stress σ_r

Load
Direction

θ

r

θ

0

.98   .97
.98
1.07
1.18
1.38
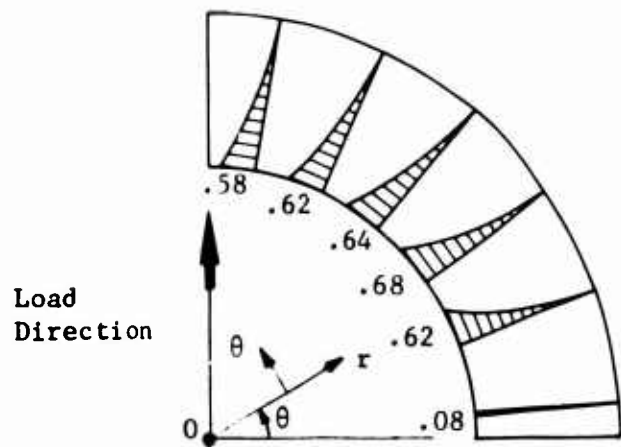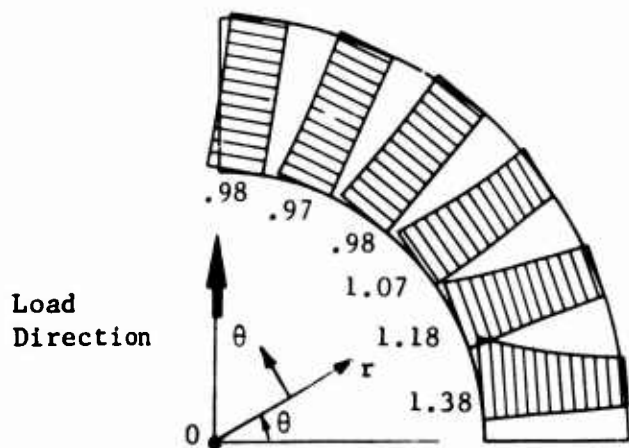
b)   Tangential stress σ_θ

Figure 14.   Stress Diagrams for Isotropic Material (Steel).

24

Load
Direction

a) Radial stress σ_r

Load
Direction
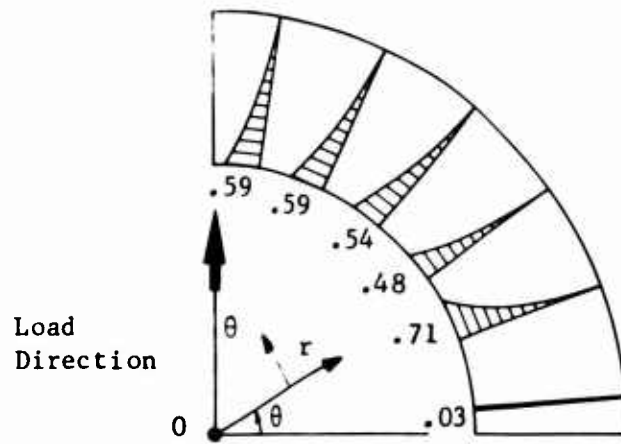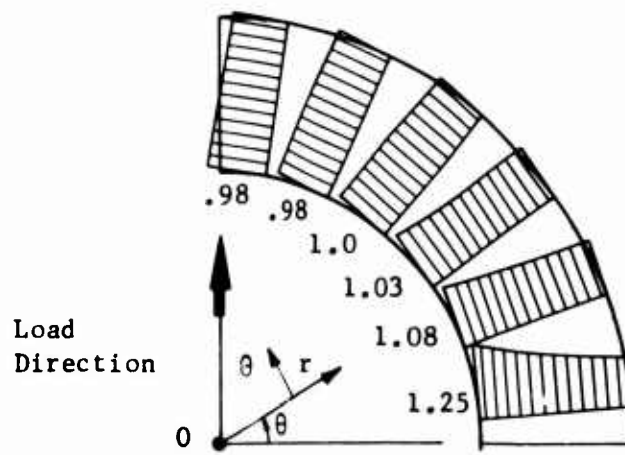
b) Tangential stress σ_θ

Figure 15. Stress Diagrams for Glass Composite Material (V_F = 0.7).

25
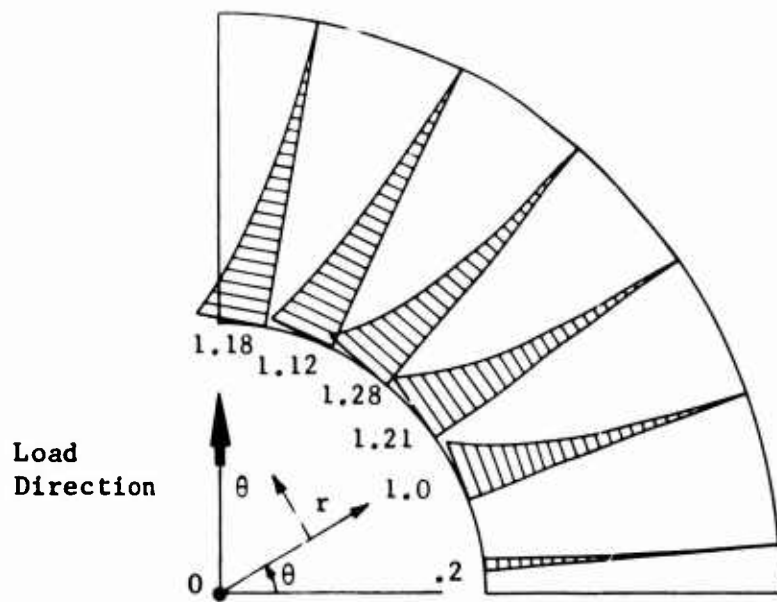
a) Radial stress σ_r

b) Tangential stress σ_θ

Figure 16. Stress Diagrams for Isotropic Material (Steel).

Load
Direction

1.20 1.15
1.22
1.20
1.19
.09

a) Radial stress σ_r

Load
Direction

.96 .98
1.02
1.11
1.19
1.36

b) Tangential stress σ_θ

Figure 17. Stress Diagrams for Glass Composite Material (V_F = 0.7).

27

Load
Direction

1.82 2.00
1.88
1.78
1.38
0.35

a) Radial stress σ_r

Load
Direction

1.11 1.29
1.25
1.39
1.61
1.78
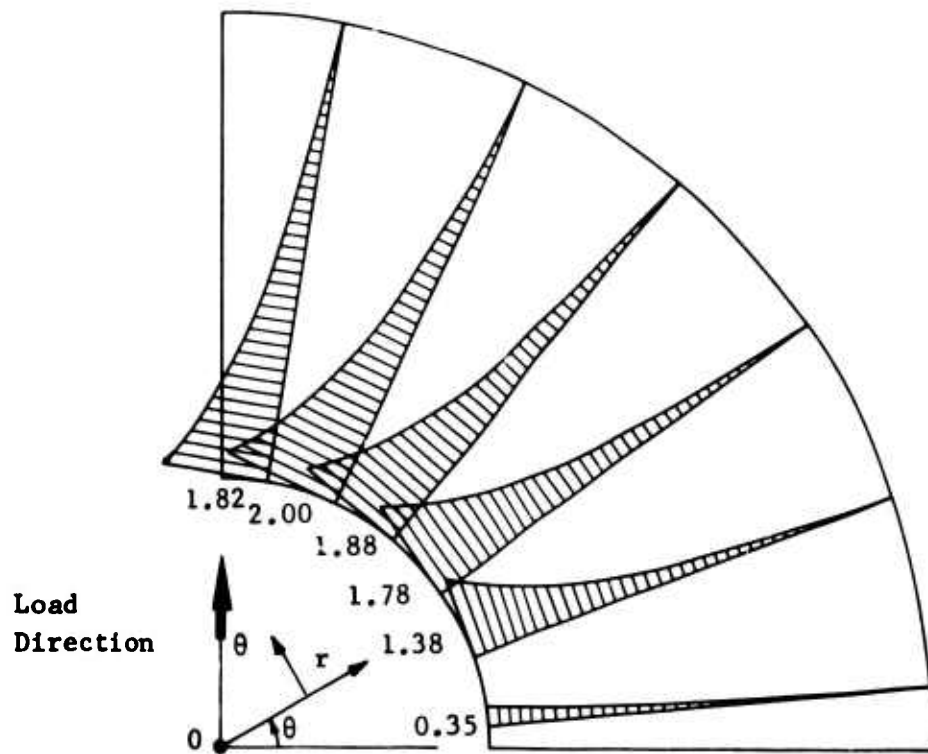
b) Tangential stress σ_θ

Figure 18. Stress Diagrams for Isotropic Material (Steel).

28
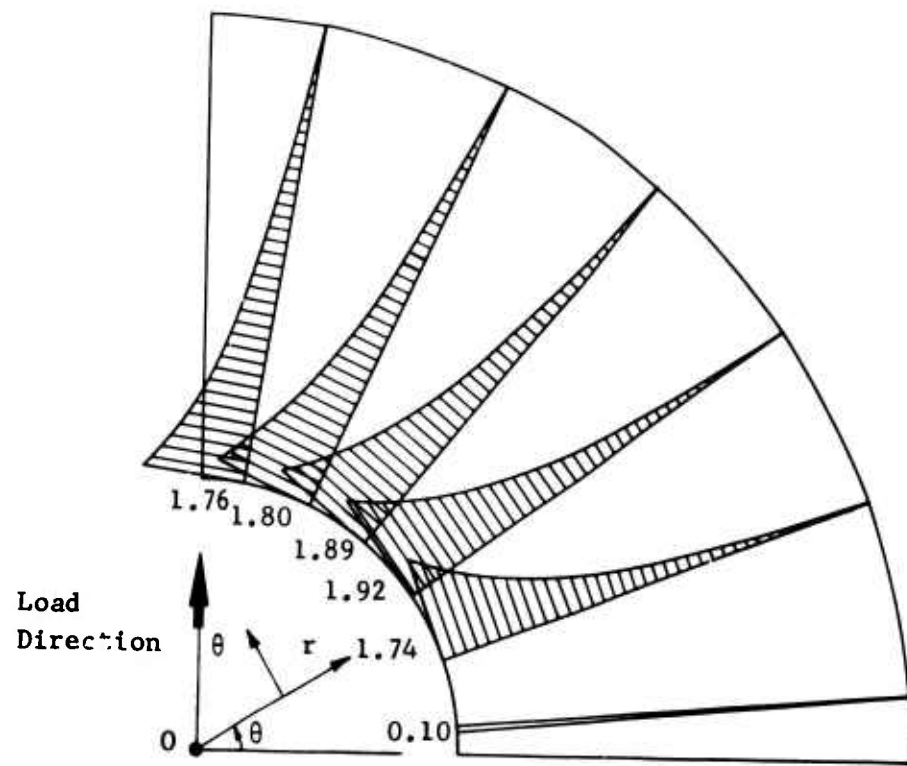
a) Radial stress σ_r
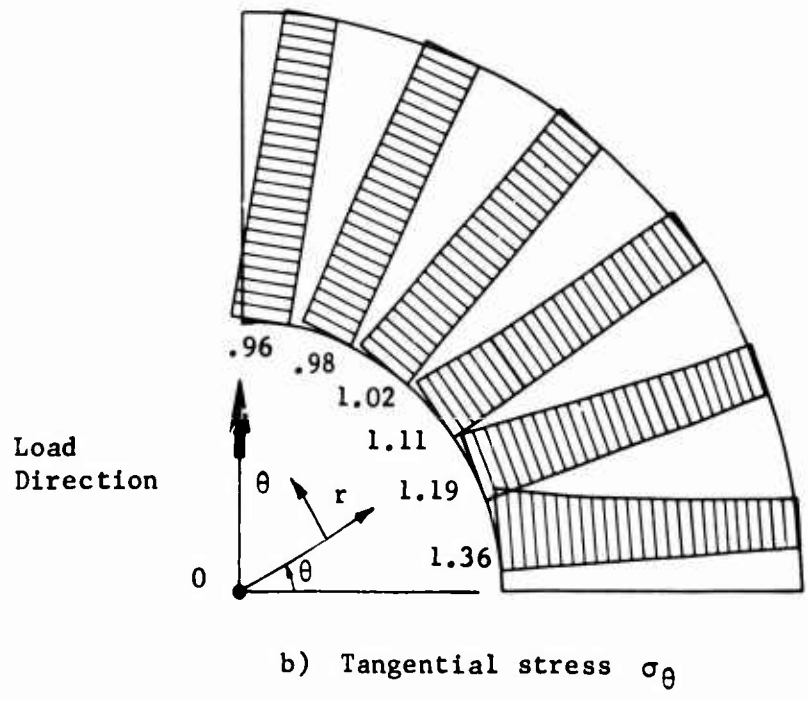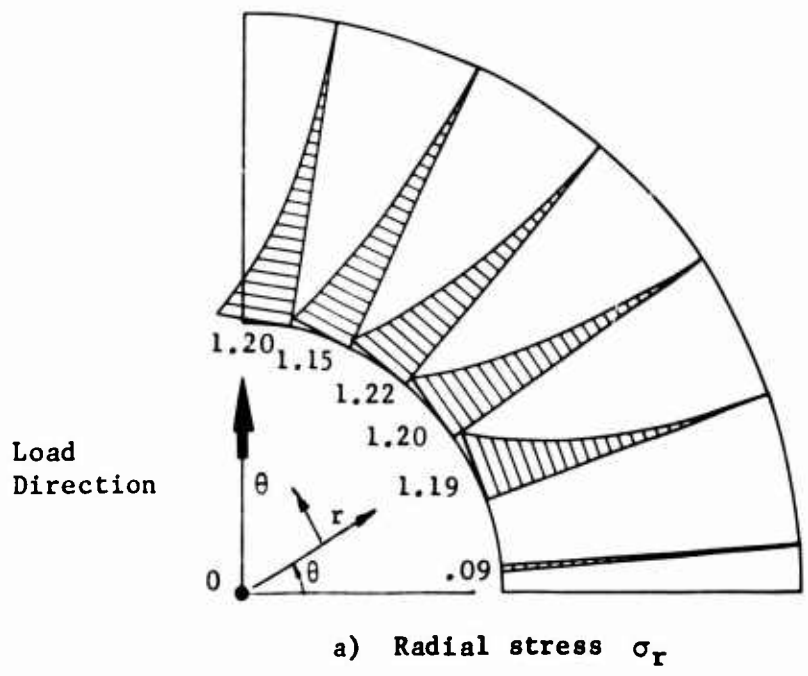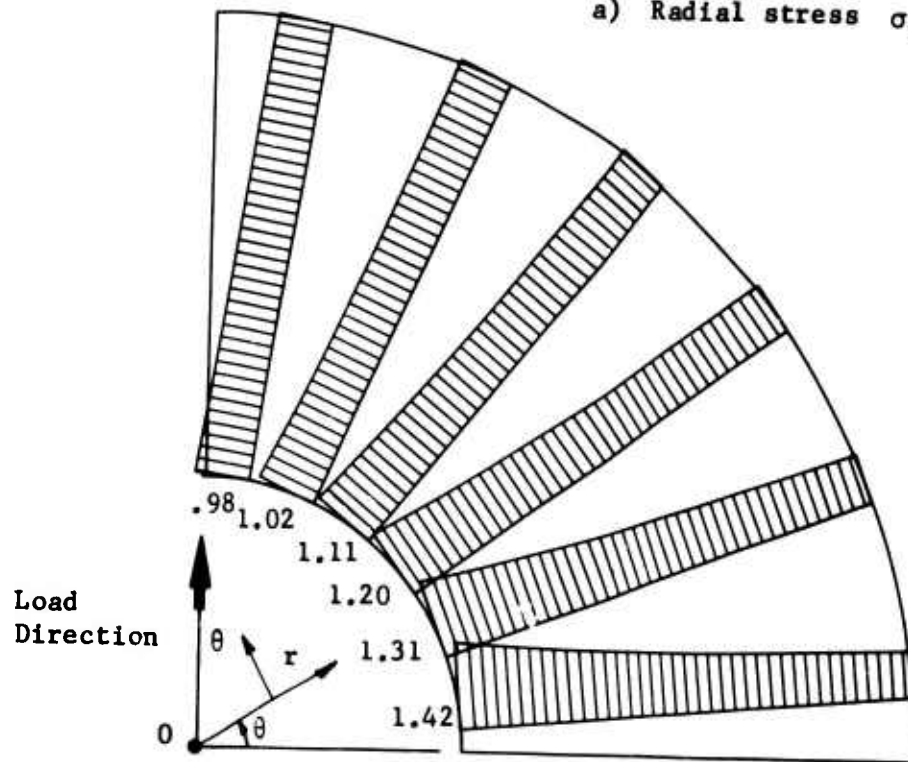
b) Tangential stress σ_θ

Figure 19. Stress Diagrams for Glass Composite Material ($V_F = 0.7$).

29

Figure 20 is a plot of the ratio $\sigma_{r(max)}/\sigma_{avg}$ against t/a, σ_{avg} being the average stress $P/2t$ and P the total applied tensile load.

This relation can be expressed with minimal error by the linear formula

$$\sigma_{r(max)} = 1.13\ \sigma_{avg}\ \frac{t}{a} \tag{54}$$

Figure 21 shows the curve of $\sigma_\theta/\sigma_{avg}$ with t/a as the independent variable. The value σ_θ is corresponding to the point in which σ_r is a maximum. This point is where the factor of safety is minimum, as we will see later. The curve of Figure 21 can be approximately expressed by the following:

$$\sigma_\theta = \left[1 + 0.079\left(\frac{t}{a}\right)^2\right]\sigma_{avg} \tag{55}$$
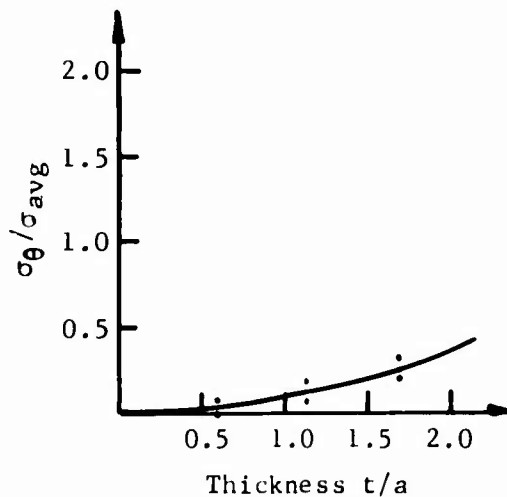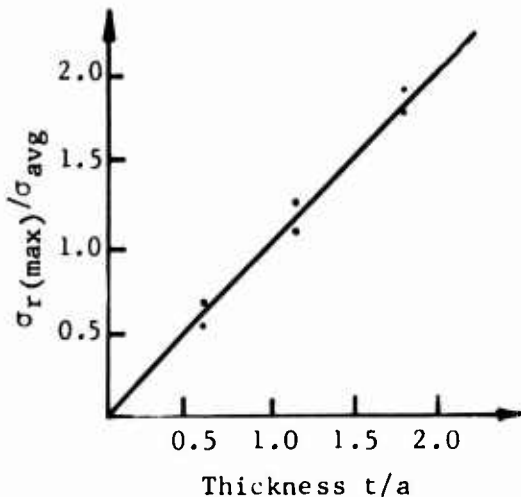
Figure 20. Maximum Radial Stress.

Figure 21. Value of σ_θ Where σ_r Is Maximum.

STRUCTURAL DESIGN OF BOLT JOINTS

Failure Criteria

Once the stress distribution is known, it is necessary to adopt a failure criterion in order to establish the factor of safety of the joint. A failure theory widely used is the so-called interaction formula[9]

$$\left(\frac{\sigma_x}{\sigma_x^*}\right)^2 - \frac{\sigma_x\sigma_y}{\sigma_x^*\sigma_y^*} + \left(\frac{\sigma_y}{\sigma_y^*}\right)^2 + \left(\frac{\tau_{xy}}{\tau_{xy}^*}\right)^2 = 1 \tag{56}$$

30

where σ_x , σ_y , and τ_{xy} are the macromechanical stresses and σ_x^* , σ_y^* , and τ_{xy}^* are the failure stresses. The normal stresses σ_x and σ_y are positive (negative) corresponding to tension (compression). The failure stress σ_x^* must be the failure stress in tension if σ_x is positive, and the failure stress in compression if σ_x is negative. The same criterion is used with respect to σ_y and σ_y^* . In the formula, σ_x^* and σ_y^* must always be positive. The interaction formula as a failure criterion was introduced in Reference 7. Other failure criteria are presented in References 11 and 12.

In the following, we will adopt the interaction formula (56) as the representative failure criterion. By referring equation (56) to the polar coordinates r and θ , and by taking into account that $\tau_{r\theta} = 0$ for the critical area of the joint, we get the factor of safety μ:

$$\mu = \frac{1}{\sqrt{\left(\dfrac{\sigma_r}{\sigma_r^*}\right)^2 - \dfrac{\sigma_r \sigma_\theta}{\sigma_r^* \sigma_\theta^*} + \left(\dfrac{\sigma_\theta}{\sigma_\theta^*}\right)^2}} \qquad (57)$$

If the joint is made in the manner indicated in Figure 22, the stress σ_r^* is the tension failure stress for the unidirectional composite in the fiber direction, and σ_θ^* is the compression failure stress in the normal direction.

Design Procedure

The design procedure for a bolt joint will be illustrated on a joint selected from the Mohawk plane of Grumman Aircraft Company. This joint corresponds to the wing-fuselage connection, and the ultimate load in tension is $P = 30,000$ lb. Information about the joint design is given in References 13, 14, and 15.
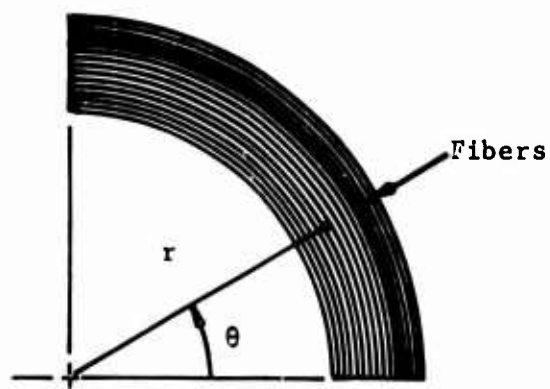
Figure 22.   Unidirectional Composite Joint.

Figure 23 shows the preliminary adopted dimensions by using glass fibers and epoxy resin with a fiber volume content of 70% to 75%.

31
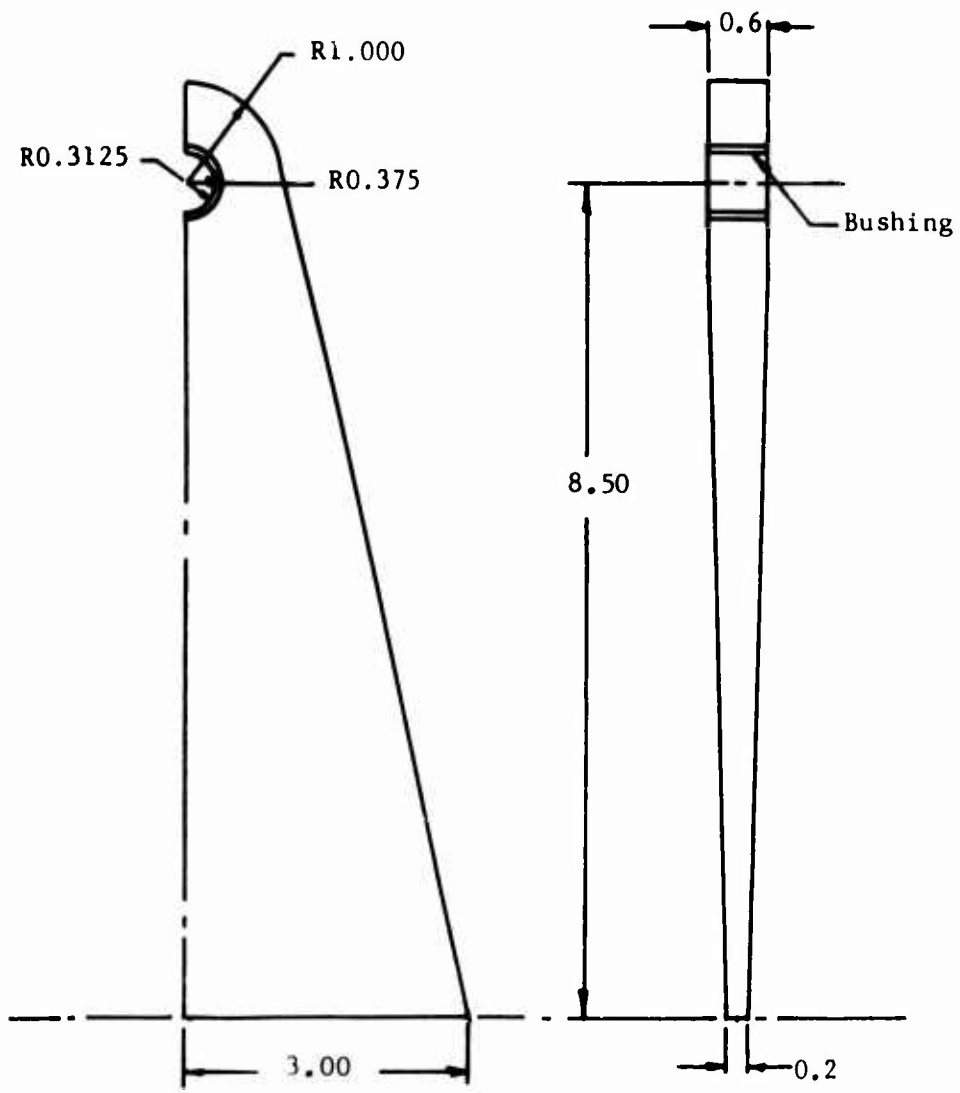
Figure 23. Dimensions of the Bolt Joint (inch).

The ratios t/a and σ_{avg} are

$$\frac{t}{a} = \frac{1.000 - 0.375}{0.375} = 1.67$$

$$\sigma_{avg} = \frac{30,000}{0.6 \cdot 0.625 \cdot 2} = 40,000 \text{ psi}$$

Then, from equations (54) and (55), we get

$$(\sigma_r)_{max} = 1.89 \, \sigma_{avg} \quad , \quad \sigma_\theta = 1.22 \, \sigma_{avg}$$

or, with the value of σ_{avg} obtained before,

$$(\sigma_r)_{max} = 75,600 \text{ psi} \quad , \quad \sigma_\theta = 48,800 \text{ psi}$$

The failure stresses for the unidirectional composite employed are

$$\sigma_r{}^* = 30,000 \text{ psi} \quad , \quad \sigma_\theta{}^* = 225,000 \text{ psi}$$

The failure stress in compression corresponds to the 0.2% limit of strain. It is not an actual 'failure stress." By using this value and on the basis of equation (57), a factor of safety of $\mu = 0.38$ results and the failure load will be

$$P^* = 0.38 \cdot 30,000 = 11,400 \text{ lb}$$

However, the failure load obtained from tests is about 26,000 lb, as shown in the discussion of experimental results in this report. This discrepancy between analytical and experimental results stems from the following fact: When the load reaches a value of 12,000 lb, a plastic area appears as shown in Figure 24, and the load-elongation diagram presents "jumps" which
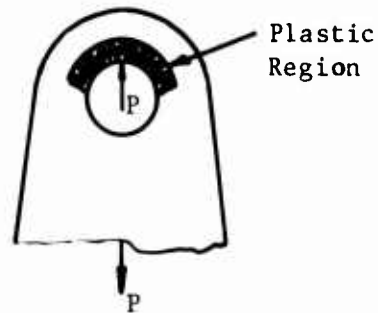
Figure 24.   Plastic Region.

33

indicate the successive progress of the plasticized area. Thus, the load obtained from the linear stress analysis only indicates the beginning of the formation of the plastic areas.

By taking bushings of larger external diameter, we can make joints of smaller ratio t/a . The following two values are considered:

$$\frac{t}{a} = 1.0 \quad , \quad \frac{t}{a} = 0.66$$

The corresponding values of μ obtained by following the same procedure as above result in the values in Table II.

TABLE II. SAFETY FACTORS		
$\dfrac{t}{a}$	1.0	0.66
σ_{avg}	50,000	62,500
$(\sigma_r)_{max}$	ɔo,500	46,600
σ_θ	53,900	64,700
μ	0.504	0.582

This shows that the factor of safety increases when t/a decreases. However, in practical applications of joints, other limitations exist that do not permit the use of a very low value of t/a . A ratio $t/a = 1$ appears to be quite adequate for most of the bolt joints of composite materials.

The ultimate failure load, which is the maximum load that can possibly be applied to the joint before it breaks completely, is approximately double the load given by the described procedure. This assumption proved to be valid only for $0.9 \le t/a \le 1.1$.

EXPERIMENTAL RESULTS

The experimental program was divided into two parts, one concerning a simple loop joint and the other the bolt joint.

Loop Joint

An experimental program concerned with the stress distribution and failure loads of loop joints was developed.

The joints tested to failure had the dimensions indicated in Figure 25.

Figure 25. Dimensions of the Loop Joint.

The specimens were made of glass composite material and were tested in tension. The load was applied by using a fixture schematically shown in Figure 26. A bushing was not used between bolt and joint, and special care was taken to ensure perfect initial contact between bolt and joint at the surface of load transference.
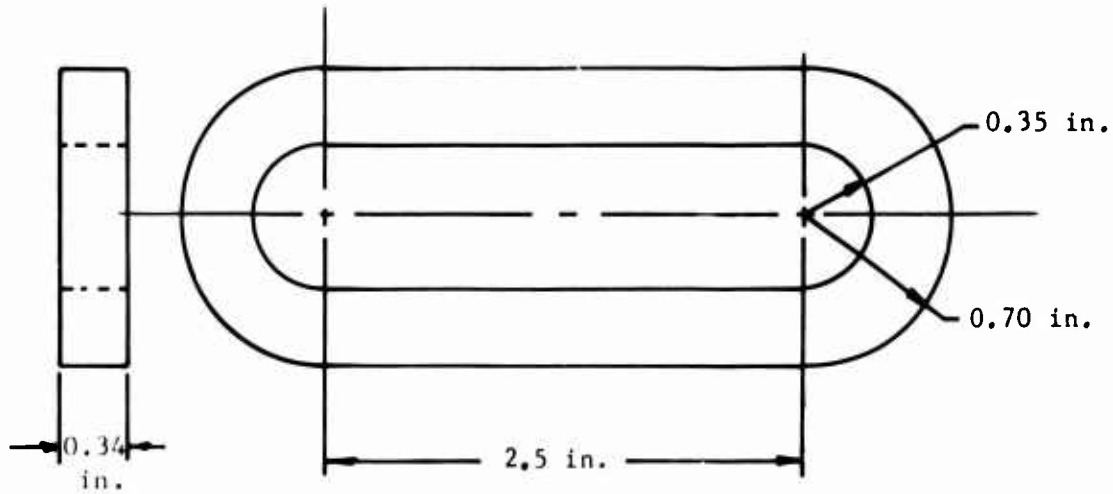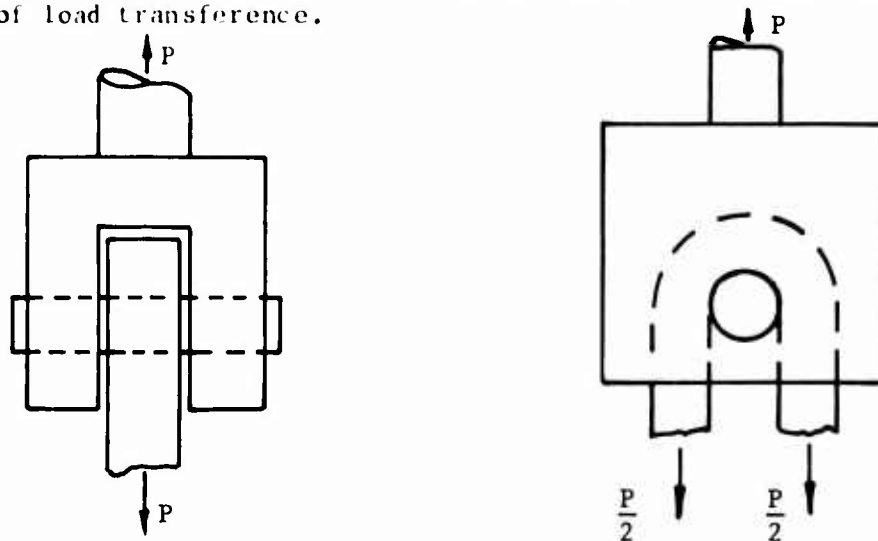
Figure 26. Attachment Device for Testing.

35

The failure loads obtained from the tests are summarized in Table III.

	TABLE III. FAILURE LOADS		
Specimen No.	Dimensions of a Simple Cross Section, in.	Failure load, lb	Avg Failure Stress, psi X 10^{-3}
1	0.342 X 0.308	12,900	61.5
2	0.346 X 0.295	11,250	55.2
3	0.344 X 0.282	10,400	53.7
4	0.348 X 0.301	13,350	63.2
5	0.346 X 0.378	13,100	52.0

The ultimate strength of the joint's material in simple tension was 150-180 kpsi. Therefore, the efficiency of the loop joint is about 0.33. In other words, the ultimate strength of the loop joint is one-third of the strength of the same material in simple tension. This conclusion is limited only to joints with a ratio $t/a = 1$.

Figures 27, 28, and 29 illustrate the location and form of failure. The regions of resin under failure (opaque areas in the photographs) encompass three-fourths of the total section. It is also possible to observe that the failure is produced for $20° < \theta < 80°$.

A failure test was performed by using a plastic homogeneous, brittle material loop joint. Figure 30 shows the failure produced.

Photoelastic studies were conducted to establish the stress distribution in both orthotropic and isotropic loop joints. Figure 31 shows the isoclines for 0°, 30°, and 60° for the isotropic joint. Similar patterns were obtained on orthotropic loop joints by using the reflection method of photoelasticity. The position of the inclines confirms the analytical results in the sense that the shear stresses $\tau_{r\theta}$ are very small. In fact, the isocline lines are approximately radial straight lines, forming angles of 0°, 30°, and 60°, respectively.
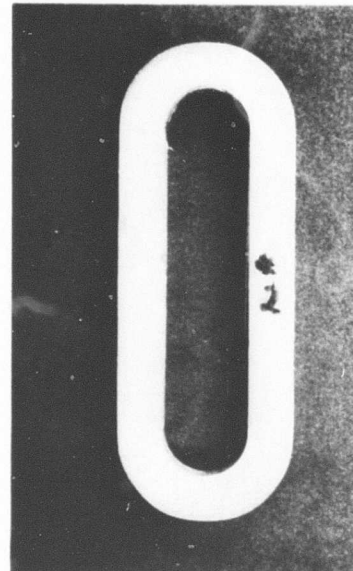
Figure 27. Loop Joint of Composite Material After Testing to Failure.
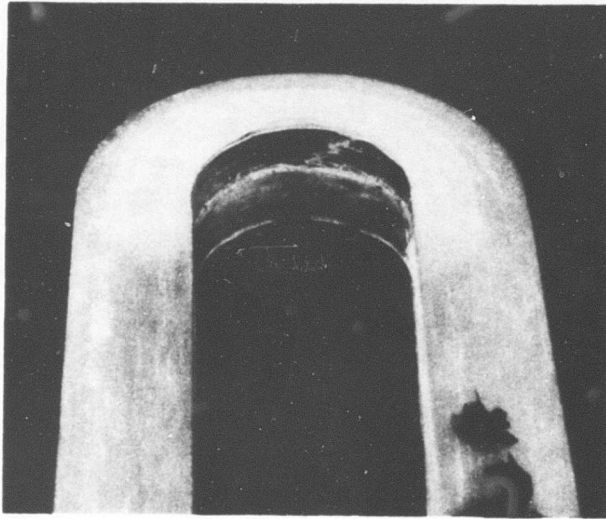
Figure 28.   Loop Joint of Composite
Material After Testing
to Failure.
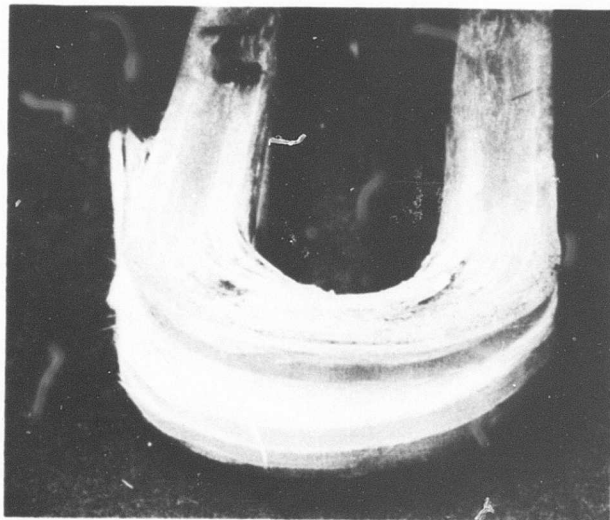
Figure 29.   Loop Joint of Composite
Material After Testing
to Failure.
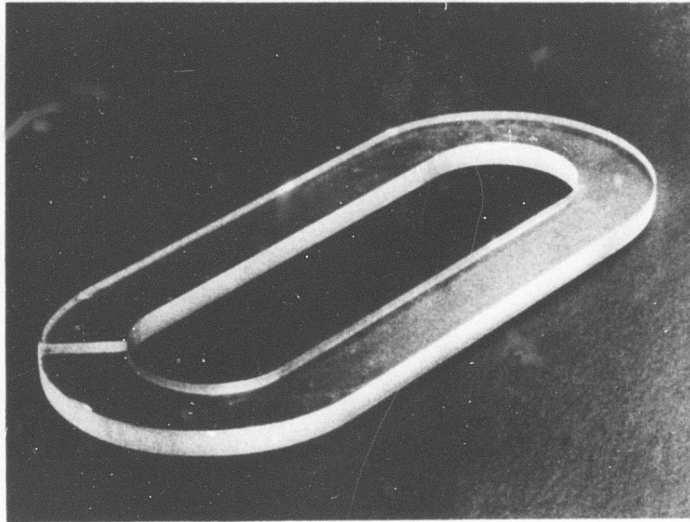
Figure 30. Failure of an Isotropic Joint of
Brittle Material.
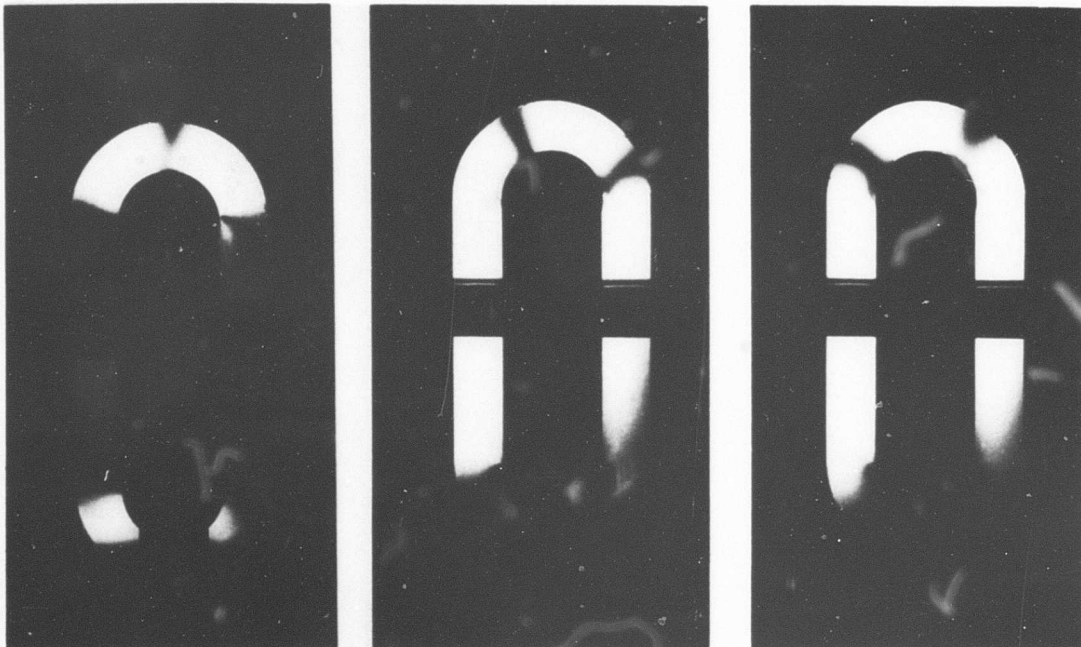
(a) Isoclines of 0°   (b) Isoclines of 30°   (c) Isoclines of 60°

Figure 31. Isoclines for 0°, 30°, and 60°
for the Isotropic Joint.

38

Bolt Joint

The tested bolt joints were similar to those shown in Figure 32. Table IV
indicates the characteristics and ultimate load of the tested bolt joints.
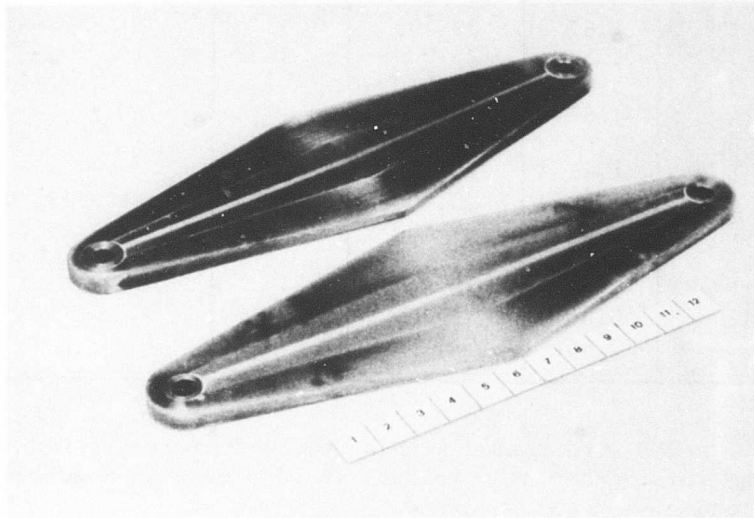
(a) Composite Joints
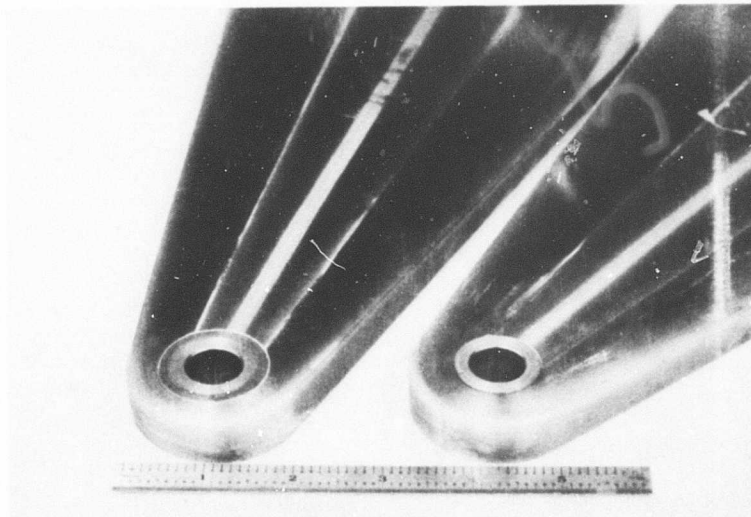
(b) Composite Joints

Figure 32.   Bolt Joints Similar to
Those Tested.

39

Specimen No.	Ratio t/a	Ultimate Load, lb	Figure No.	Observations
				TABLE IV. SPECIMEN CHARACTERISTICS AND ULTIMATE LOADS

TABLE IV. SPECIMEN CHARACTERISTICS AND ULTIMATE LOADS

Specimen No.	Ratio t/a	Ultimate Load, lb	Figure No.	Observations
1	1.67	29,700	33	--
2	1.67	25,000	34	--
3	1.67	24,500	--	--
4	1.67	28,100	--	--
5	1.67	26,700	--	--
6	1.67	25,900	--	--
7	1.00	45,400	35	Laterally Supported
8	1.00	44,500	--	Laterally Supported
9	1.00	39,400	36	--
10	1.00	38,800	--	--
11	0.66	42,200	37	--
12	0.66	41,500	--	--

Specimens 7 and 8 were tested with a device that restricted lateral expansion of the joint under high loads. In this way, an increment of the ultimate load of 10% was obtained.
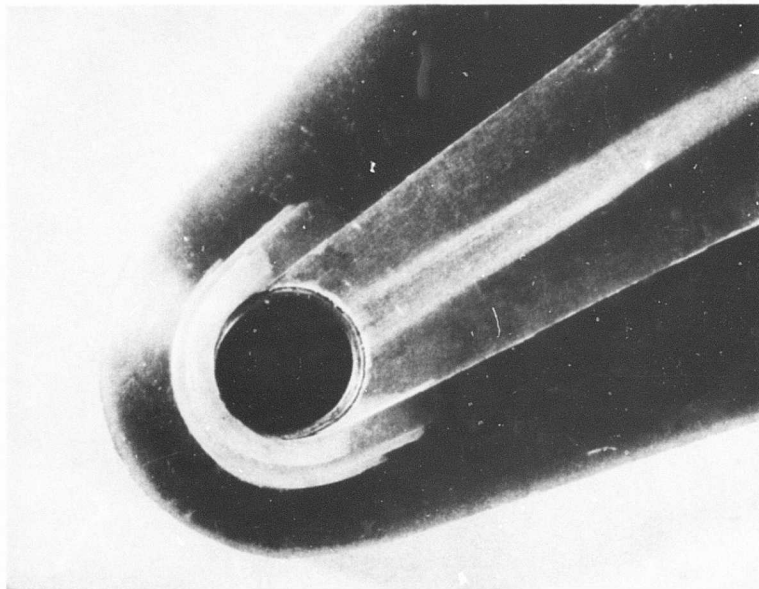
Figure 33. Composite Joint After Failure.
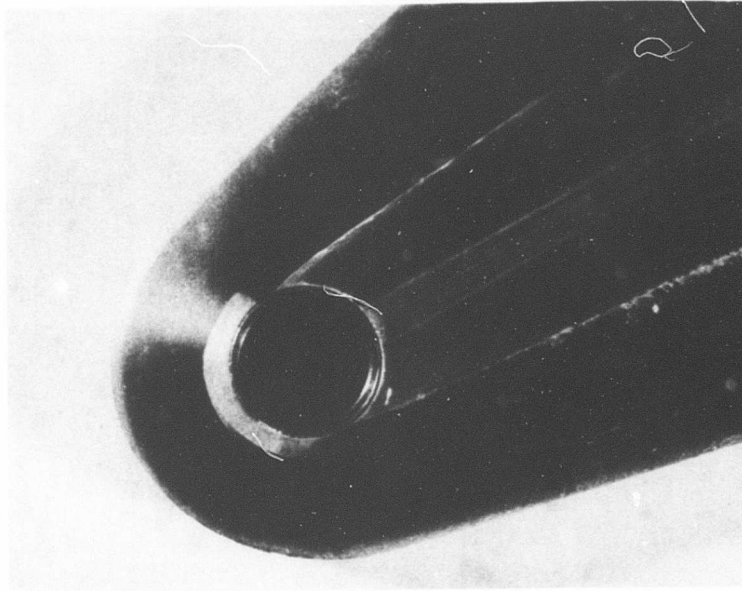
Figure 34. Composite Joint After Failure.
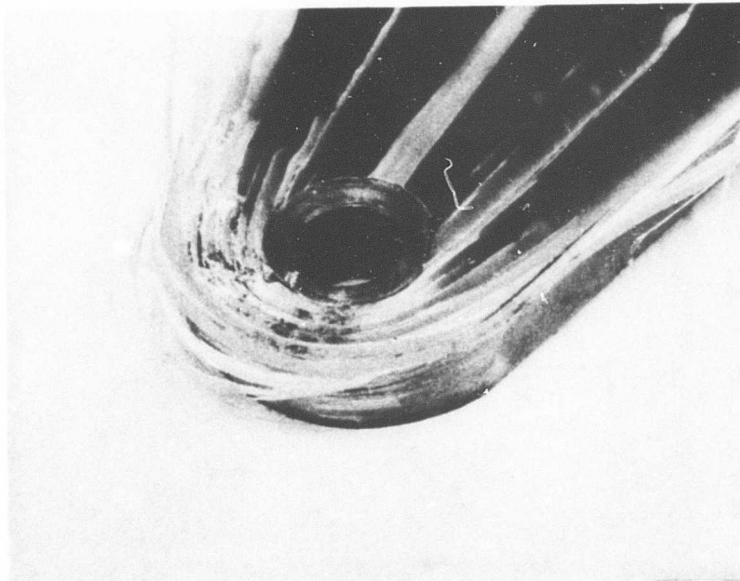
Figure 35. Composite Joint After Failure.

41
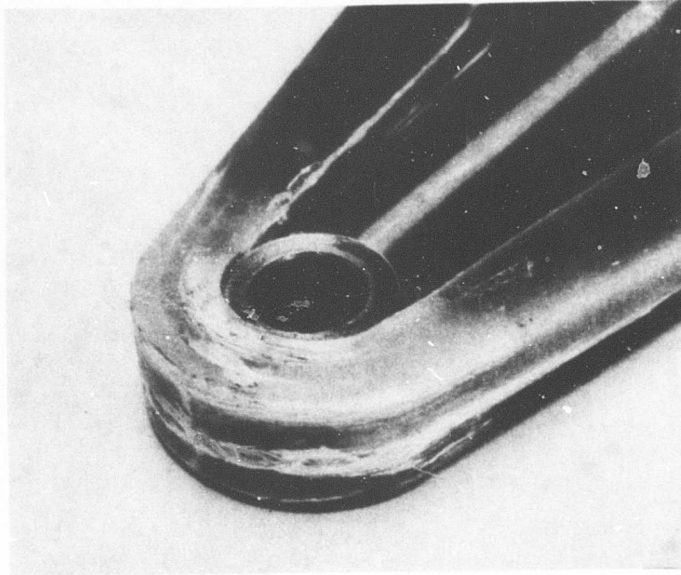
Figure 36. Composite Joint After Failure.
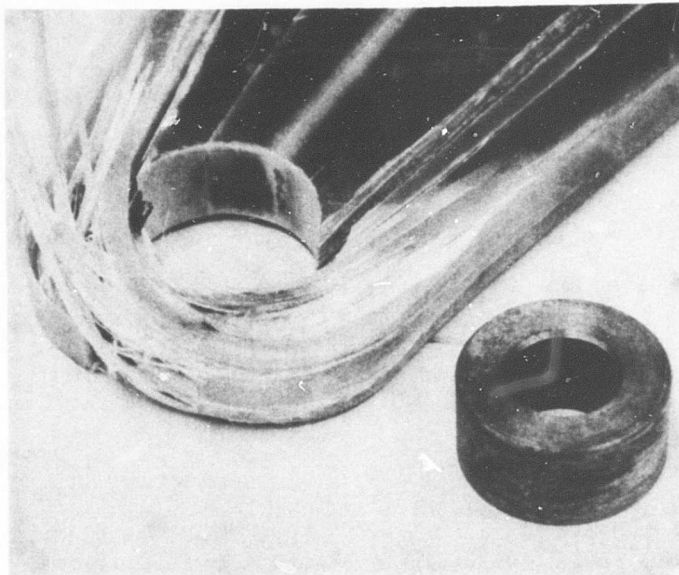
Figure 37. Composite Joint After Failure.

Figure 38 represents a typical load-displacement curve obtained during the
tension test of the bolt joints. It can be observed that there are several
"jumps" which correspond to several steps of failure that occurred during
the test. The ultimate load shown in Table IV is the highest, after which
the joint breaks.
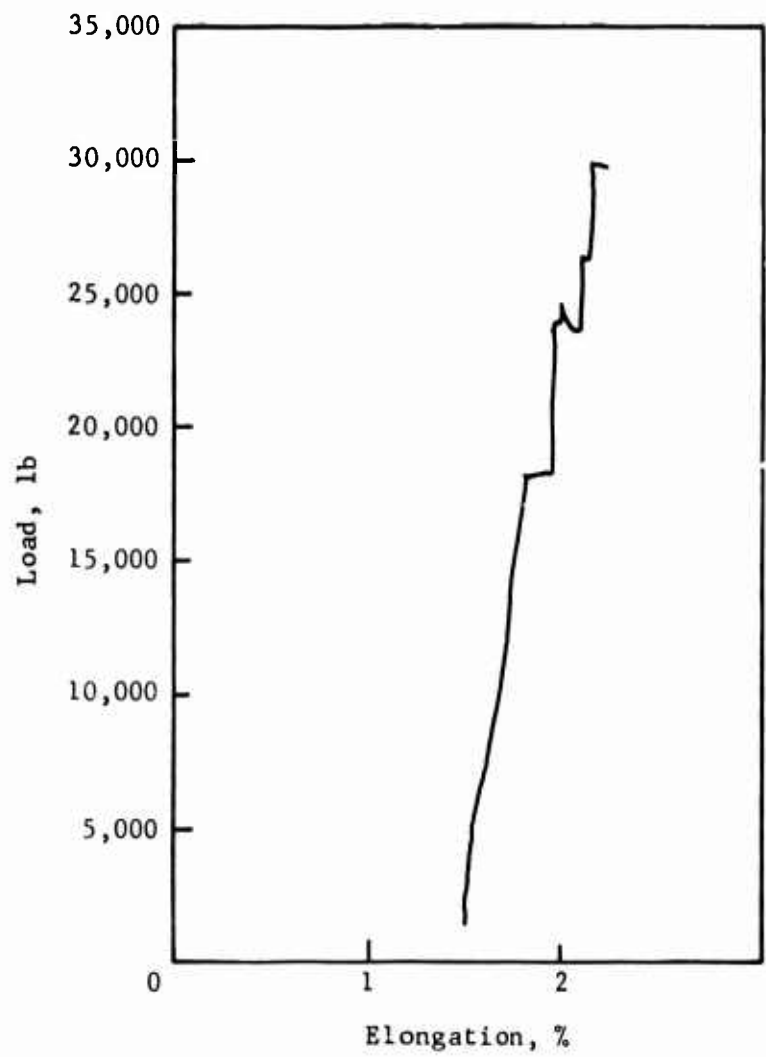
Figure 38. Testing Machine Load-Displacement
Plotted.

43

Figure 39 shows the specimen mounted in the testing machine for tension testing.

FABRICATION PROCESS

The following procedure was adhered to in the fabrication of test specimens for this program.

Material

1. 12 End Roving 5994 Glass

2. Resin System

   a. Epon 828 50 phr
   b. Epon 1031 50 phr
   c. NMA (methyl endomethylene tetrahydro phthalic anhydride catalyst) 90 phr
   d. Benzyldimethylamine (BDHA accelerator) 0.50 phr
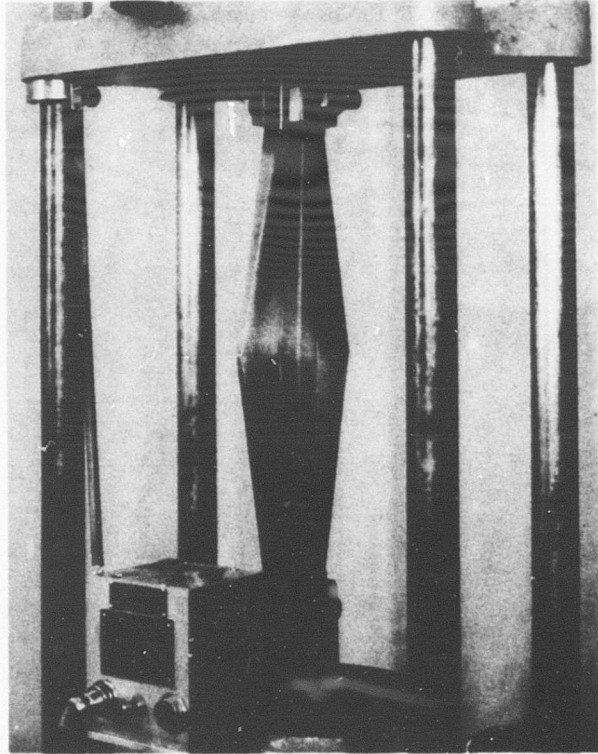
Figure 39. Specimen Mounted in the Test Machine.

Tooling

   Winding Tool (igure 40), Aluminum-Constructed Material

Equipment

1. Temperature Controlled Hot-Melt Coater

2. Fiber Tensioning Device

3. Winding Machine (special throat-deep; see Figure 41)

   a. Traverse-Controlled
   b. Revolution Infinite Control

Winding Procedure

1. Set winding traverse to 0.600 in. to yield 9 revolutions per layer.

2. Set fiber tensioning device at 2-pound fiber tension.

3. Regulate hot-melt coater temperature to 170°-180°F.

4. Preheat winding fixture to 160-180°F.

44
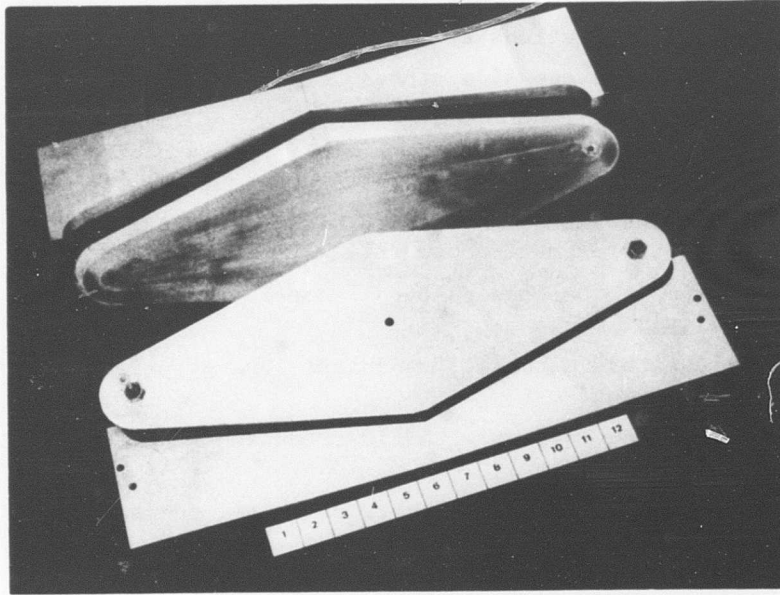
Figure 40.   Aluminum-Constructed Winding Tool.
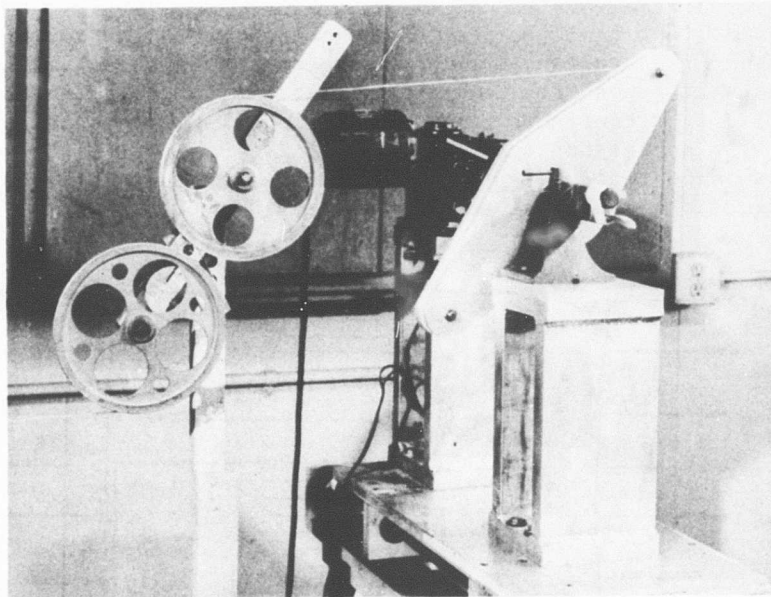
Figure 41.   Winding Machine.

5. Wind 568 revolutions at 2-pound fiber tension.

6. Apply first-stage side plates; close side plates to within 0.062 in. to stops.

7. Place assembly in a 225°F regulated press platen; close side plates just short of resin gelation.

8. Raise temperature to 250°F, reside for 1 hour at 250°F, and cure at 325°F for 1 hour. Allow to cool under pressure.

9. Disassemble tool and remove precured first-stage laminate from tool.

10. Remove excess material; sandblast faying surface for second-stage winding.

11. Wind 500 revolutions with fiber tension reduced to 1.5 pounds. Total winding revolutions of 1035.

12. Repeat operations 6 through 9 using second-stage side plates.

13. Remove part from tool and report all physical properties.

STRESS CONCENTRATION AROUND CIRCULAR HOLES IN ORTHOTROPIC PLATES

General Formulas

The technical importance of the stress concentration around holes is well known. The concentration factors have been established for the most important cases that appear for isotropic materials in technical applications. For example, in a tensioned plate with a circular hole, a diagram of stresses σ_x appears as shown in Figure 42. It is possible to see that the stress concentration factor is 3, because the peak of stress is three times larger than that of the applied stress.
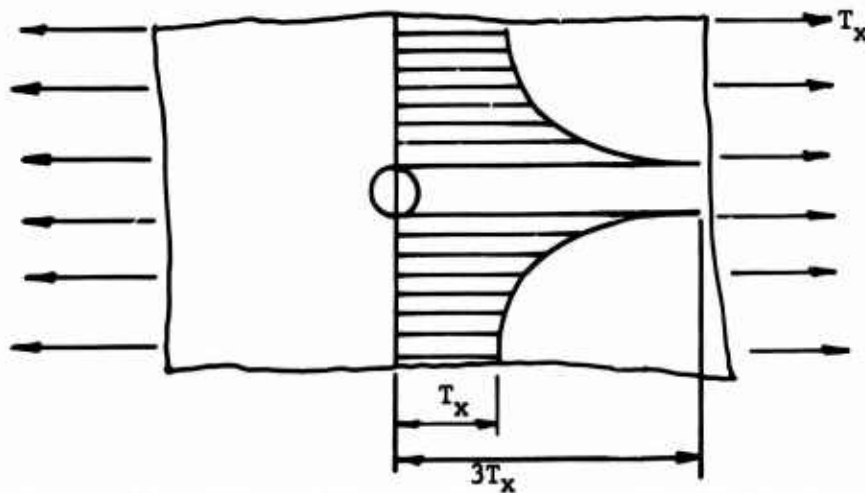
Figure 42.   Stress Concentration in Isotropic Sheet.

46

For the correct use of structural composite materials, it is important to know the influence of the relative volume and directions of the fibers on the concentration factors. This is of fundamental importance in the case of a structure with alternative loads, because the maximum stress concentration points are the origin of the failure lines.

In this part of the report, we will develop the analytical elements and a computer program that will permit us to find the concentration factors in an orthotropic plate with a circular hole. As external loads, we consider tension and pure shear. By combining the results of these two cases, it is possible to solve almost all states of stresses, assuming that the hole's diameter is small with respect to the dimensions on the middle plane of the plate.

The theoretical elements of the complex solution of the plane state of stresses are taken from Reference 16.

The fundamental differential equation of an orthotropic plate in plane stress is

$$b_{11} \frac{\partial^4 \Phi}{\partial y^4} + (2b_{12} + b_{33}) \frac{\partial^4 \Phi}{\partial x^2 \partial y^2} + b_{22} \frac{\partial^4 \Phi}{\partial x^4} = 0 \tag{58}$$

where b_{11}, b_{12}, b_{22}, and b_{33} are the elements of the matrix that connects stresses and strains; i.e.,

$$\begin{Bmatrix} \varepsilon_x \\ \varepsilon_y \\ \gamma_{xy} \end{Bmatrix} = \begin{bmatrix} b_{11} & b_{12} & 0 \\ b_{12} & b_{22} & 0 \\ 0 & 0 & b_{33} \end{bmatrix} \begin{Bmatrix} \sigma_x \\ \sigma_y \\ \tau_{xy} \end{Bmatrix}$$

It must be noted that the matrix b_{ij} is the inverse of matrix [C] mentioned earlier in this report, if this matrix also belongs to an orthotropic plate.

It is possible to rewrite this equation in the following form:

$$\left(\frac{\partial^2}{\partial x^2} + \alpha_1 \frac{\partial^2}{\partial y^2} \right) \left(\frac{\partial^2}{\partial x^2} + \alpha_2 \frac{\partial^2}{\partial y^2} \right) \Phi = 0 \tag{59}$$

with the constants α_1 and α_2 defined by

$$\alpha_1 \alpha_2 = \frac{b_{11}}{b_{22}} \quad , \quad \alpha_1 + \alpha_2 = \frac{2b_{12} + b_{33}}{b_{22}} \tag{60}$$

47

In other words, α_1 and α_2 are the roots of the equation in α

$$b_{22} \, \alpha^2 - (2b_{12} + b_{33}) \, \alpha + b_{11} \; = \; 0 \qquad (61)$$

It is possible to demonstrate by energy considerations that the roots of equation (61) are real and positive if the coefficients b_{11}, b_{12}, b_{22}, and b_{33} correspond to any orthotropic material.

Taking the complex variable $z = x + iy$ and its conjugate $\bar{z} = x - iy$, we put the stress function in the following form:

$$\Phi \; = \; f(z + \gamma_1 \bar{z}) + g \, (z + \gamma_2 \bar{z}) \qquad (62)$$

Substituting this function into the differential equation (58), we can establish that the real part of equation (62) is a solution if γ_1 and γ_2 are given by

$$\gamma_1 \; = \; \frac{\sqrt{\alpha_1} - 1}{\sqrt{\alpha_1} + 1} \qquad , \qquad \gamma_2 \; = \; \frac{\sqrt{\alpha_2} - 1}{\sqrt{\alpha_2} + 1} \qquad (63)$$

Because α_1 and α_2 are real and positive, γ_1 and γ_2 lie between -1 and 1.

Remembering that the stresses are

$$\sigma_x \; = \; \frac{\partial^2 \Phi}{\partial y^2} \quad ; \quad \sigma_y \; = \; \frac{\partial^2 \Phi}{\partial x^2} \quad ; \quad \tau_{xy} \; = \; -\frac{\partial^2 \Phi}{\partial x \partial y} \qquad (64)$$

By substitution of equation (62), we obtain

$$\sigma_x \; = \; -(1 - \gamma_1)^2 \, f''(z + \gamma_1 \bar{z}) - (1 - \gamma_2)^2 \, g''(z + \gamma_2 \bar{z})$$

$$\sigma_y \; = \; (1 + \gamma_1)^2 \, f''(z + \gamma_1 \bar{z}) + (1 + \gamma_2)^2 \, g''(z + \gamma_2 \bar{z})$$

$$\tau_{xy} \; = \; -i(1 - \gamma_1^2) \, f''(z + \gamma_1 \bar{z}) - i(1 - \gamma_2^2) \, g''(z + \gamma_2 \bar{z}) \qquad (65)$$

Introducing the function $\psi = \psi(x,y)$ by

$$\frac{\partial^2 \psi}{\partial x \partial y} \; = \; \nabla_1^2 \Phi \qquad , \qquad \frac{\partial^2 \psi}{\partial x^2} + \alpha_1 \, \alpha_2 \, \frac{\partial^2 \psi}{\partial y^2} \; = \; (1 - \alpha_1)(1 - \alpha_2) \, \frac{\partial^2 \Phi}{\partial x \partial y} \qquad (66)$$

48

the displacements are given by

$$u_x = (b_{12} - b_{22}) \frac{\partial \Phi}{\partial x} + b_{11} \frac{\partial \Psi}{\partial y}$$

$$u_y = (b_{12} - b_{22}) \frac{\partial \Phi}{\partial y} + b_{22} \frac{\partial \Psi}{\partial x} \tag{67}$$

From equations (62) and (66), it is possible to obtain

$$\frac{\partial \Psi}{\partial x} = -\frac{4i\gamma_1}{1 - \gamma_1} f'(z + \gamma_1 \bar{z}) - \frac{4i\gamma_2}{1 - \gamma_2} g'(z + \gamma_2 \bar{z})$$

$$\frac{\partial \Psi}{\partial y} = \frac{4\gamma_1}{1 + \gamma_1} f'(z + \gamma_1 \bar{z}) + \frac{4\gamma_2}{1 + \gamma_2} g'(z + \gamma_2 \bar{z}) \tag{68}$$

With equations (62) and (68), the displacements given in equation (67) become

$$u_x = (1 + \gamma_1)(b_{12} - \alpha_2 b_{22}) f'(z + \gamma_1 \bar{z})$$

$$+ (1 + \gamma_2)(b_{12} - \alpha_1 b_{22}) g'(z + \gamma_2 \bar{z})$$

$$u_y = i(1 - \gamma_1)(b_{12} - \alpha_1 b_{22}) f'(z + \gamma_1 \bar{z}) +$$

$$+ i(1 - \gamma_2)(b_{12} - \alpha_2 b_{22}) g'(z + \gamma_2 \bar{z}) \tag{69}$$

Stress function (62) must produce single-valued stresses, which tend to zero at infinity. Also, the displacements must be single-valued. These conditions are satisfied by taking as function Φ the real part of

$$\Phi = f(z + \gamma_1 \bar{z}) + \{A(1 - \gamma_2)(b_{12} - \alpha_2 b_{22})$$

$$+ iB(1 + \gamma_2)(b_{12} - \alpha_1 b_{22})\} (z + \gamma_1 \bar{z}) \ln(z + \gamma_1 \bar{z})$$

$$+ g(z + \gamma_1 \bar{z}) - \{A(1 - \gamma_1)(b_{12} - \alpha_1 b_{22})$$

$$+ iB(1 + \gamma_1)(b_{12} - \alpha_2 b_{22})\} (z + \gamma_2 \bar{z}) \ln(z + \gamma_2 \bar{z}) \tag{70}$$

where A and B are real constants.

49

The stresses corresponding to the function (70) are obtained by using equations (64):

$$\sigma_x = -(1 - \gamma_1)^2 \left\{ f''(z + \gamma_1\overline{z}) + [A(1 - \gamma_2)(b_{12} - \alpha_2 b_{22}) \right.$$
$$\left. + iB(1 + \gamma_2)(b_{12} - \alpha_1 b_{22})] \frac{1}{z + \gamma_1\overline{z}} \right\}$$
$$- (1 - \gamma_2)^2 \left\{ g''(z + \gamma_2\overline{z}) - [A(1 - \gamma_1)(b_{12} - \alpha_1 b_{22}) \right.$$
$$\left. + iB(1 + \gamma_1)(b_{12} - \alpha_2 b_{22})] \frac{1}{z + \gamma_2\overline{z}} \right\}$$

$$\sigma_y = (1 + \gamma_1)^2 \left\{ f''(z + \gamma_1\overline{z}) + [A(1 - \gamma_2)(b_{12} - \alpha_2 b_{22}) \right.$$
$$\left. + iB(1 + \gamma_2)(b_{12} - \alpha_1 b_{22})] \frac{1}{z + \gamma_1\overline{z}} \right\}$$
$$+ (1 + \gamma_2)^2 \left\{ g''(z + \gamma_2\overline{z}) - [A(1 - \gamma_1)(b_{12} - \alpha_1 b_{22}) \right.$$
$$\left. + iB(1 + \gamma_1)(b_{12} - \alpha_2 b_{22})] \frac{1}{z + \gamma_2\overline{z}} \right\}$$

$$\tau_{xy} = -i(1 - \gamma_1^2) \left\{ f''(z + \gamma_1\overline{z}) + [A(1 - \gamma_2)(b_{12} - \alpha_2 b_{22}) \right.$$
$$\left. + iB(1 + \gamma_2)(b_{12} - \alpha_1 b_{22})] \frac{1}{z + \gamma_1\overline{z}} \right\}$$
$$- (1 - \gamma_2^2) \left\{ g''(z + \gamma_2\overline{z}) - [A(1 - \gamma_1)(b_{12} - \alpha_1 b_{22}) \right.$$
$$\left. + iB(1 + \gamma_1)(b_{12} - \alpha_2 b_{22})] \frac{1}{z + \gamma_2\overline{z}} \right\} \tag{71}$$

Now we introduce the two new functions of the complex variable

$$z = re^{i\theta} \tag{72}$$

defined by the integral forms

$$P = \frac{1}{2\pi} \int_0^{2\pi} \frac{ze^{-i\theta} + a}{ze^{-i\theta} - a} (\sigma_r)_{r=a} \, d\theta$$

50

$$Q = \frac{i}{2\pi} \int_0^{2\pi} \frac{ze^{-i\theta} + a}{ze^{-i\theta} - a} (\tau_{r\theta})_{r=a} \, d\theta \tag{73}$$

From these equations, it is possible to see that the functions P and Q are related to the tractions on the boundary of the circular hole. In these equations, θ is the angular coordinate of the point on the boundary $r=a$ in which the stresses σ_r and $\tau_{r\theta}$ are taken. The functions P and Q are finite at infinity and

$$\{Re[P]\}_{r=a} = -(\sigma_r)_{r=a}$$

$$\{Im[Q]\}_{r=a} = -(\tau_{r\theta})_{r=a} \tag{74}$$

Substituting equations (71) into the transformation formulas

$$\sigma_r = \sigma_x \cos^2 \theta + \sigma_y \sin^2 \theta + 2\tau_{xy} \sin \theta \cos \theta$$

$$\tau_{r\theta} = (\sigma_y - \sigma_x) \sin \theta \cos \theta + \tau_{xy} (\cos^2 \theta - \sin^2 \theta) \tag{75}$$

we obtain the polar components of the stresses:

$$\sigma_r = -\frac{(z - \gamma_1 \bar{z})^2}{z\bar{z}} \left\{ f''(z + \gamma_1 \bar{z}) + [A(1 - \gamma_2)(b_{12} - \alpha_2 b_{22}) \right.$$
$$\left. + iB(1 + \gamma_2)(b_{12} - \alpha_1 b_{22})] \frac{1}{z + \gamma_1 \bar{z}} \right\}$$
$$- \frac{(z - \gamma_2 \bar{z})^2}{z\bar{z}} \left\{ g''(z + \gamma_2 \bar{z}) - [A(1 - \gamma_1)(b_{12} - \alpha_1 b_{22}) \right.$$
$$\left. + iB(1 + \gamma_1)(b_{12} - \alpha_2 b_{22})] \frac{1}{z + \gamma_2 \bar{z}} \right\}$$

$$\tau_{r\theta} = -\frac{i(z^2 - \gamma_1^2 \bar{z}^2)}{z\bar{z}} \left\{ f''(z + \gamma_1 \bar{z}) + [A(1 - \gamma_2)(b_{12} - \alpha_2 b_{22}) \right.$$
$$\left. + iB(1 + \gamma_2)(b_{12} - \alpha_1 b_{22})] \frac{1}{z + \gamma_2 \bar{z}} \right\} -$$

(continued)

51

$$- \frac{i(z - \gamma_2^2 \bar{z}^2)}{z\bar{z}} \left\{ g''(z + \gamma_2 \bar{z}) - [A(1 - \gamma_1)(b_{12} - \alpha_1 b_{22}) \right.$$

$$\left. + iB(1 + \gamma_1)(b_{12} - \alpha_2 b_{22})] \frac{1}{z + \gamma_2 \bar{z}} \right\} \quad (76)$$

By putting these stresses into equations (74), functions P and Q become

$$P = \frac{1}{a^2} \left[z - \left(\frac{\gamma_1 a^2}{z} \right)^2 \right] f'' \left[z + \left(\frac{\gamma_1 a^2}{z} \right) \right] + \frac{1}{a^2} \left(z - \frac{\gamma_2 a^2}{z} \right) g'' \left(z + \frac{\gamma_2 a^2}{z} \right)$$

$$+ A(1 - \gamma_2)(b_{12} - \alpha_2 b_{22}) \left(\frac{1 + \gamma_1}{z} - \frac{4\gamma_1}{z + \frac{\gamma_1 a^2}{z}} \right)$$

$$- iB(1 + \gamma_2)(b_{12} - \alpha_1 b_{22}) \left(\frac{1 - \gamma_1}{z} + \frac{4\gamma_1}{z + \frac{\gamma_1 a^2}{z}} \right)$$

$$- A(1 - \gamma_1)(b_{12} - \alpha_1 b_{22}) \left(\frac{1 + \gamma_2}{z} - \frac{4\gamma_2}{z + \frac{\gamma_2 a^2}{z}} \right)$$

$$- iB(1 + \gamma_1)(b_{12} - \alpha_2 b_{22}) \left(\frac{1 - \gamma_2}{z} + \frac{4\gamma_2}{z + \frac{\gamma_2 a^2}{z}} \right)$$

$$Q = \frac{1}{a^2} \left(z^2 - \frac{\gamma_1^2 a^4}{z^2} \right) f'' \left(z + \frac{\gamma_1 a^2}{z} \right) - \frac{1}{a^2} \left(z^2 - \frac{\gamma_2^2 a^4}{z^2} \right) g'' \left(z + \frac{\gamma_2 a^2}{z} \right)$$

$$+ (A + iB)[(1 + \gamma_1)(1 - \gamma_2)(b_{12} - \alpha_2 b_{22})$$

$$- (1 - \gamma_1)(1 + \gamma_2)(b_{12} - \alpha_1 b_{22})] \frac{1}{z} \quad (77)$$

Now we define the two new variables ξ and η by the following equations:

$$z = \frac{1}{2} \xi \left[1 + \left(1 - \frac{4\gamma_1 a^2}{\xi^2} \right)^{\frac{1}{2}} \right] \quad , \quad z = \frac{1}{2} \eta \left[1 + \left(1 - \frac{4\gamma_2 a^2}{\eta^2} \right)^{\frac{1}{2}} \right] \quad (78)$$

The variable z must be single-valued. Therefore, the arguments of the complex expressions $1 - 4\gamma_1 a^2/\xi^2$ and $1 - 4\gamma_1 a^2/\eta^2$ must be between $-\pi$ and π.

Combining equations (77) and (78), we get

$$(\gamma_1 - \gamma_2)\left(1 - \frac{4\gamma_1 a^2}{\xi^2}\right)^{\frac{1}{2}} [\xi f''(\xi) + A(1 - \gamma_2)(B_{12} - \alpha_2 b_{22})$$

$$+ iB(1 + \gamma_2)(b_{12} - \alpha_1 b_{22})] = A(1 - \gamma_2)^2(b_{12} - \alpha_2 b_{22})$$

$$- A(1 - \gamma_1)(1 - \gamma_2)(b_{12} - \alpha_1 b_{22}) - iB(1 + \gamma_2)^2(b_{12} - \alpha_1 b_{22})$$

$$+ iB(1 + \gamma_1)(1 + \gamma_2)(b_{12} - \alpha_2 b_{22})$$

$$- \frac{\xi}{4}[P(\xi) + Q(\xi)]\left[1 + \left(1 - \frac{4\gamma_1 a^2}{\xi^2}\right)^{\frac{1}{2}}\right]$$

$$- \frac{\gamma_2 \xi}{4\gamma_1}[P(\xi) - Q(\xi)]\left[1 - \left(1 - \frac{4\gamma_1 a^2}{\xi^2}\right)^{\frac{1}{2}}\right] \qquad (79)$$

$$(\gamma_1 - \gamma_2)\left(1 - \frac{4\gamma_2 a^2}{\eta^2}\right)^{\frac{1}{2}} [\eta g''(\eta) - A(1 - \gamma_1)(b_{12} - \alpha_1 b_{22})$$

$$- iB(1 + \gamma_1)(b_{12} - \alpha_2 b_{22})] = A(1 - \gamma_1)^2(b_{12} - \alpha_1 b_{22})$$

$$- A(1 - \gamma_1)(1 - \gamma_2)(b_{12} - \alpha_2 b_{22}) - iB(1 + \gamma_1)^2(b_{12} - \alpha_2 b_{22})$$

$$+ iB(1 + \gamma_1)(1 + \gamma_2)(b_{12} - \alpha_1 b_{22})$$

$$+ \frac{\eta}{4}[P(\eta) + Q(\eta)]\left[1 + \left(1 - \frac{4\gamma_2 a^2}{\eta^2}\right)^{\frac{1}{2}}\right]$$

$$+ \frac{\gamma_1 \eta}{4\gamma_2}[P(\eta) - Q(\eta)]\left[1 - \left(1 - \frac{4\gamma_2 a^2}{\eta^2}\right)^{\frac{1}{2}}\right] \qquad (80)$$

53

For a particular problem, functions P and Q can be computed by using equations (74), because $(\sigma_r)_{r=a}$ and $(\tau_{r\theta})_{r=a}$ are known from the boundary conditions. By integration of the stresses on the boundary of the hole, we find the resultant forces

$$X = 2\pi A(1 - \gamma_1)(1 - \gamma_2)(\alpha_1 - \alpha_2)b_{22}$$

$$Y = 2\pi B(1 + \gamma_1)(1 + \gamma_2)(\alpha_1 - \alpha_2)b_{22} \tag{81}$$

Equations (73) can be used to find $V(z)$ and $W(z)$, and by solving equations (81), constants A and B can be established. Then, from equations (79) and (80), we obtain $f''(\xi)$ and $g''(\eta)$. The stresses are given by equations (71), where we now have

$$\xi = z + \gamma_1\bar{z} \quad , \quad \eta = z + \gamma_2\bar{z} \tag{82}$$

Stress Concentration for Pure Tension

The tension load T_x is applied at the x direction, as shown in Figure 43.
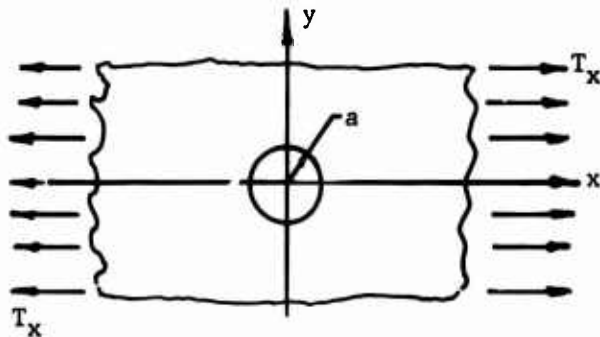

Figure 43. Tension Load Applied
at the x Direction.

If there is no hole in the plate, the stresses are

$$\sigma_x = T_x \quad , \quad \sigma_y = 0 \quad , \quad \tau_{xy} = 0 \tag{83}$$

or, in polar coordinates, according to the formulas (75),

$$\sigma_r = \frac{T_x}{2}(1 + \cos 2\theta)$$

54

$$\sigma_\theta = \frac{T_x}{2}(1 - \cos 2\theta)$$

$$\tau_{r\theta} = -\frac{T_x}{2}\sin 2\theta \qquad (84)$$

It is now necessary to find a stress system which tends to zero at the infinite and which takes the values

$$(\sigma_r)_s = -\frac{T_x}{2}(1 + \cos 2\theta)$$

$$(\sigma_\theta)_s = -\frac{T_x}{2}(1 - \cos 2\theta)$$

$$(\tau_{r\theta})_s = \frac{T_x}{2}\sin 2\theta \qquad (85)$$

when $r = a$

Thus, from equations (73), we get

$$P = \frac{T_x}{2}\left(1 + \frac{a^2}{z^2}\right) \quad , \quad Q = -\frac{T_x}{2}\left(1 - \frac{a^2}{z^2}\right) \qquad (86)$$

With the variables ξ and η introduced by equations (78), we obtain the following from equations (84):

$$P(\xi) - Q(\xi) = P(\eta) - Q(\eta) = T$$

$$P(\xi) + Q(\xi) = \frac{T_x\left\{1 - \left(1 - \dfrac{4\gamma_1 a^2}{\xi^2}\right)^{\frac{1}{2}}\right\}}{\gamma_1\left\{1 + \left(1 - \dfrac{4\gamma_1 a^2}{\xi^2}\right)^{\frac{1}{2}}\right\}}$$

$$P(\eta) + Q(\eta) = \frac{T_x\left\{1 - \left(1 - \dfrac{4\gamma_2 a^2}{\eta^2}\right)^{\frac{1}{2}}\right\}}{\gamma_2\left\{1 + \left(1 - \dfrac{4\gamma_2 a^2}{\eta^2}\right)^{\frac{1}{2}}\right\}} \qquad (87)$$

55

Because the stresses in equation (85) do not produce a resultant force on the hole, constants A and B are zero, as equations (81) demonstrate. Thus, from equations (79) and (80), and by taking into account equations (77) and (87), we get

$$f''(\xi) = \frac{T_x(1 + \gamma_2)}{4\gamma_1(\gamma_1 - \gamma_2)}\left\{1 - \left(1 - \frac{4\gamma_1 a^2}{\xi^2}\right)^{-\frac{1}{2}}\right\}$$

$$g''(\eta) = -\frac{T_x(1 + \gamma_1)}{4\gamma_2(\gamma_1 - \gamma_2)}\left\{1 - \left(1 - \frac{4\gamma_2 a^2}{\eta^2}\right)^{-\frac{1}{2}}\right\} \tag{88}$$

Using these equations and remembering equations (82), then the following stresses result from equations (71):

$$\sigma_x = \frac{(1 + \gamma_1)(1 + \gamma_2)T_x}{4\gamma_1\gamma_2} + \frac{T_x}{4(\gamma_1 - \gamma_2)}\left\{\frac{(1 + \gamma_2)(1 - \gamma_1)^2}{\gamma_1 X_1}\right.$$
$$\left. - \frac{(1 + \gamma_1)(1 - \gamma_2)^2}{\gamma_2 X_2}\right\}$$

$$\sigma_y = -\frac{(1 + \gamma_1)(1 + \gamma_2)T_x}{4\gamma_1\gamma_2} - \frac{T_x}{4(\gamma_1 - \gamma_2)}\left\{\frac{(1 + \gamma_2)(1 + \gamma_1)^2}{\gamma_1 X_1}\right.$$
$$\left. - \frac{(1 + \gamma_1)(1 + \gamma_2)^2}{\gamma_2 X_2}\right\}$$

$$\tau_{xy} = \frac{iT_x}{4(\gamma_1 - \gamma_2)}\left\{\frac{(1 + \gamma_2)(1 - \gamma_1^2)}{\gamma_1 X_1} - \frac{(1 + \gamma_1)(1 - \gamma_2^2)}{\gamma_2 X_2}\right\} \tag{89}$$

where the following notation was used:

$$X_1 = R_1^{\frac{1}{2}} e^{\frac{i\Phi_1}{2}} \quad , \quad X_2 = R_2^{\frac{1}{2}} e^{\frac{i\Phi_2}{2}} \tag{90}$$

with

$$R_1 e^{i\Phi_1} = 1 - \frac{4a^2\gamma_1}{(z + \gamma_1 \bar{z})^2} \quad , \quad R_2 e^{i\Phi_2} = 1 - \frac{4a^2\gamma_2}{(z + \gamma_2\bar{z})^2} \tag{91}$$

56

The quantities R_1 and R_2 are chosen as positive, and Φ_1 and Φ_2 are to lie between $-\pi$ and π. Also, it must be emphasized that the actual stresses are the real part of complex expressions (89).

Stress Concentration for Pure Shear

A shear load T_{xy} is applied on the plate with the circular hole, as shown in Figure 44. If the hole is absent, the stresses are

$$\sigma_x = 0 \quad , \quad \sigma_y = 0 \quad , \quad \tau_{xy} = T_{xy} \tag{92}$$

or, in polar coordinates,

$$\sigma_r = T_{xy} \sin 2\theta$$

$$\sigma_\theta = -T_{xy} \sin 2\theta$$

$$\tau_{r\theta} = T_{xy} \cos 2\theta \tag{93}$$
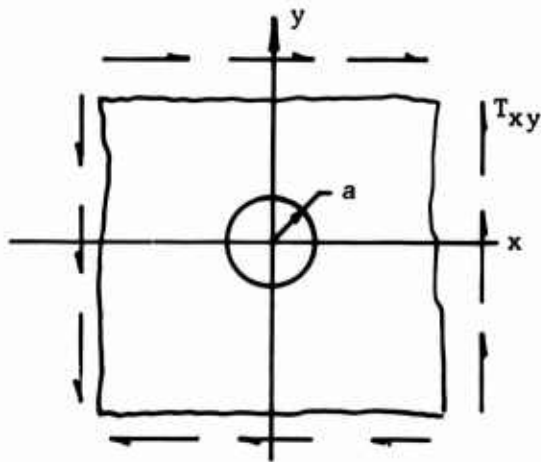

Figure 44. Shear Load Applied on
Plate With Circular Hole.

Thus, to keep the hole boundary free of stresses, it is necessary to sum to the stresses (93), the stresses which take the values

$$(\sigma_r)_s = -T_{xy} \sin 2\theta \quad , \quad (\tau_{r\theta})_s = -T_{xy} \cos 2\theta \tag{94}$$

on the hole and zero at the infinite.

57

By using equations (73), we obtain

$$P = Q = T_{xy} \frac{ia^2}{z^2} \tag{95}$$

and, from equations (84),

$$P(\xi) - Q(\xi) = P(\eta) - Q(\eta) = 0 \tag{96}$$

$$P(\xi) + Q(\xi) = \frac{2i\,T_{xy}\left\{1 - \left(1 - \frac{4\gamma_1 a^2}{\xi^2}\right)^{\frac{1}{2}}\right\}}{\gamma_1\left\{1 + \left(1 - \frac{4\gamma_1 a^2}{\xi^2}\right)^{\frac{1}{2}}\right\}}$$

$$P(\eta) + Q(\eta) = \frac{2i\,T_{xy}\left\{1 - \left(1 - \frac{4\gamma_2 a^2}{\eta^2}\right)^{\frac{1}{2}}\right\}}{\gamma_2\left\{1 + \left(1 - \frac{4\gamma_2 a^2}{\eta^2}\right)^{\frac{1}{2}}\right\}} \tag{97}$$

The constants A and B of equations (81) are zero because the resultant force (X, Y) on the hole is zero. With equations (96) and (97), from equations (79) and (80), we have

$$f''(\xi) = \frac{i\,T_{xy}}{2\gamma_1(\gamma_1 - \gamma_2)}\left\{1 - \left(1 - \frac{4\gamma_1 a^2}{\xi^2}\right)^{-\frac{1}{2}}\right\}$$

$$g''(\eta) = \frac{i\,T_{xy}}{2\gamma_2(\gamma_1 - \gamma_2)}\left\{1 - \left(1 - \frac{4\gamma_2 a^2}{\eta^2}\right)^{\frac{1}{2}}\right\} \tag{98}$$

With these results and with equations (82), from equations (71) the stresses are the real part of the expressions

$$\sigma_x = \frac{i\,T_{xy}}{2(\gamma_1 - \gamma_2)}\left\{\frac{(1 - \gamma_1)^2}{\gamma_1 X_1} - \frac{(1 - \gamma_2)^2}{\gamma_2 X_2}\right\}$$

$$\sigma_y = -\frac{i\,T_{xy}}{2(\gamma_1 - \gamma_2)}\left\{\frac{(1 + \gamma_1)^2}{\gamma_1 X_1} - \frac{(1 + \gamma_2)^2}{\gamma_2 X_2}\right\} \tag{99}$$

58

$$\tau_{xy} = \frac{\gamma_1 \gamma_2 - 1}{2\gamma_1 \gamma_2} T_{xy} - \frac{T_{xy}}{2(\gamma_1 - \gamma_2)} \left\{ \frac{1 - \gamma_1^2}{\gamma_1 X_1} - \frac{1 - \gamma_2^2}{\gamma_2 X_2} \right\} \qquad (100)$$

The meaning of X_1 and X_2 is given in equations (90) and (91).

Numerical Results

By using equations (89) and (99), it is possible to study the stress concentration around a circular hole on an orthotropic plate under axial and shear loads. A computer program based on these complex expressions was developed.

A representative value of the stress concentration originated by a circular hole is the stress $(\sigma_x)_m$ at the point A when the applied load produces unit stress in the plate without a hole. By using the computer program, we obtained the results plotted in Figure 45. It can be observed that the maximum stress concentration factor is obtained when the axial load is applied in the direction of the fibers (x , in this case).
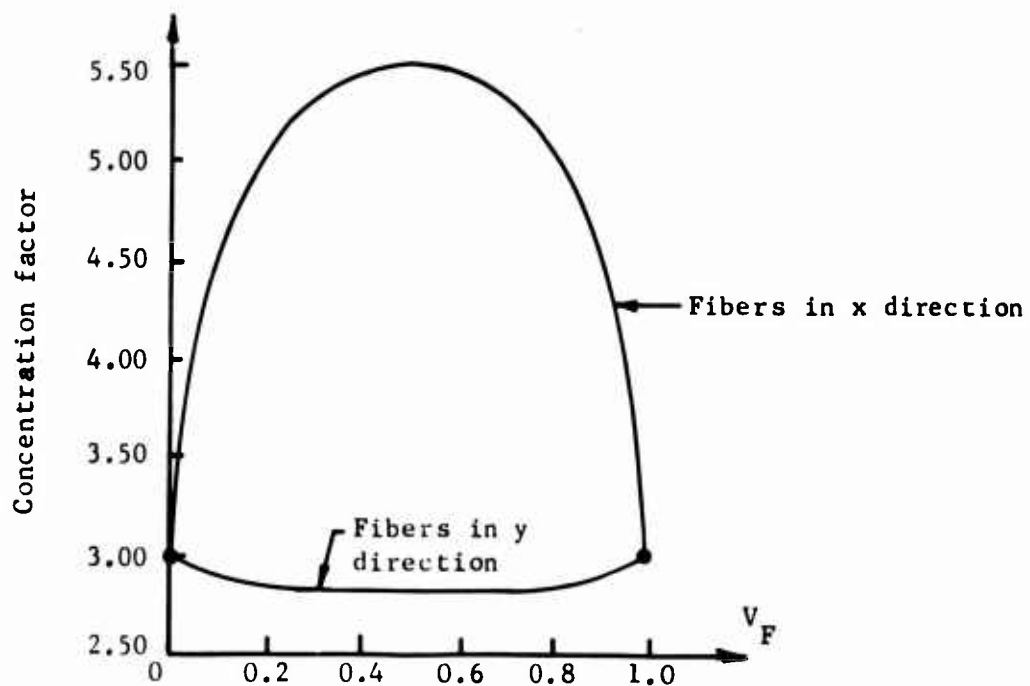

Figure 45. Stress Concentrations (maximum stresses σ_{xm}) in a Unidirectional Composite With a Circular Hole.

59

The magnitude of the concentration factor indicates that this phenomenon is more critical than in the isotropic materials, where the factor is only 3.

It must be noted that this analysis is based on the hypothesis that the material constants do not depend on x and y. To satisfy this condition, the hole must be made by cutting the fibers as indicated in Figure 46.
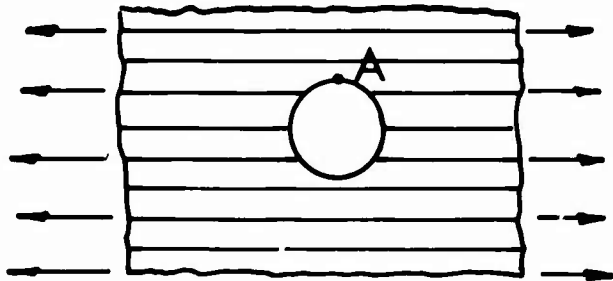
Figure 46. Orthotropic Sheet.

A more rational form for the fibers is shown in Figure 47, where fibers are not cut. The corresponding stress analysis cannot be performed with expressions (89) and (99) because now the elastic constants change from point to point. In other words, the material is not quasi-homogeneous. However, the stress analysis of this case can be made by using the method developed on page 46.

Figure 47. Nonorthotropic Sheet.

60

The numerical study was performed for unidirectional composites, in which the importance of the stress concentration factor is more evident. However, formulas (89) and (99) can also be applied for multilayered composite materials by considering the adequate constants b_{ij} .

CONCLUSIONS AND RECOMMENDATIONS

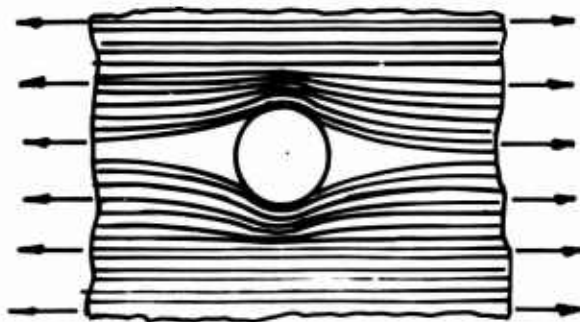The introduction of localized high loads into a thin sheet can be accomplished effectively by the use of bolt joints; contrary to the metallic joints, there are no discontinuities present when joints made of filamentary composites are used. A further advantage of filamentary joints is their behavior when loaded to failure. For example, after the first break occurs, the joint can still be loaded to almost twice the failure load. Since the first break is very easily detectable, it is possible to avoid continuation of a catastrophic failure and still maintain the load-carrying capability of a structure.

The stress analysis of composite joints, as presented herein, shows that an effective safety factor can be obtained that is within the accuracy demanded by technical requirements.

In a circular form cutout in a unidirectional composite, the stresses can reach values twice as high as those attained in an isotropic material if the fibers terminate in the rim of the cutout. For this reason, it is recommended that the fibers be led in a continuous manner around the cutout as far as fabrication requirements permit. Impelled by the great potentials of composite joints, further studies of other shapes of joints and types of loadings are recommended.

62

REFERENCES CITED

1. Haener, J. A., and N. Ashbaugh, THREE-DIMENSIONAL STRESS DISTRIBUTION IN A UNIDIRECTIONAL COMPOSITE, Journal of Composite Materials, Vol. 12, No. 1, January 1967.

2. Haener, J. A., A. H. Puppo, and Ming-Yuan Feng, OBLIQUE LOADING OF UNIDIRECTIONAL FIBER COMPOSITES; SHEAR LOADING, Whittaker Research & Development/San Diego; USAAVLABS Technical Report 68-81, U. S. Army Aviation Materiel Laboratories, Fort Eustis, Virginia, January 1969.

3. Haener, J. A., A. H. Puppo, and Ming-Yuan Feng, TRANSVERSE LOADING OF A COMPOSITE, Whittaker Research & Development/San Diego; U. S. Army Aviation Materiel Laboratories, Fort Eustis, Virginia (in preparation).

4. Argyris, J. H., RECENT ADVANCES IN MATRIX METHODS OF STRUCTURAL ANALYSIS, The MacMillan Company, New York, 1964.

5. MATRIX METHODS IN STRUCTURAL MECHANICS, Proceedings of the 1965 Conference, Air Force Flight Dynamics Laboratory Report AFFDL-TR-66-80, Wright-Patterson Air Force Base, Ohio, October 1965.

6. Ault, R. M., and L. M. Lackman, SOLUTIONS TO MIXED BOUNDARY VALUE PROBLEMS OF ORTHOTROPIC SHEETS, Report NA-67-25, North American Aviation, Los Angeles, California, 1967.

7. Hearmon, R. F. S., AN INTRODUCTION TO APPLIED ANISOTROPIC ELASTICITY, Oxford-at-the-Clarendon Press, England, 1961.

8. Lackman, L. M., and R. M. Ault, MOLLIFYING STRESS FIELDS BY USING FILAMENTARY COMPOSITE MATERIALS, Paper D-3, presented to the 12th National SAMPE Symposium, October 10-12, 1967.

9. Tsai, S. W., STRENGTH CHARACTERISTICS OF COMPOSITE MATERIALS, Philco Corporation, Aeronutronic Division; NASA Report CR-224, National Aeronautics and Space Administration, April 1965.

10. Norris, C. B., STRENGTH OF ORTHOTROPIC MATERIALS SUBJECTED TO COMBINED STRESS; FPL Report 1816, US Department of Agriculture, Forest Products Laboratory, Madison, Wisconsin, 1962.

11. Hoffman, O., THE BRITTLE STRENGTH OF ORTHOTROPIC MATERIALS, Journal of Composite Materials, Vol. 1, 1967.

12. Puppo, A. H., NEW FAILURE THEORY FOR COMPOSITE MATERIALS, Technical Note TN-68.64, Whittaker Research & Development/San Diego, California, 1968.

13. Cozzone, F. P., M. A. Maelcon, and F. M. Hoblit, ANALYSIS OF LUGS AND SHEAR PINS MADE OF ALUMINUM OR STEEL ALLOYS, Product Engineering, May 1950.

14. Conen, H., DEFORMATION UND VERSAGEN VON GFK-STRANGSCHLAUFEN, Kunstoffe, Bd. 56, Heft 9, 1966.

15. Hütter, V., PROBLEME DER KRAFTEINLEITUNG IN GLASFASER-KUNSTOFF-BAUTEILE, Kunstoffe, Bd. 53, 1963.

16. Green, A. E., and W. Zerna, THEORETICAL ELASTICITY, McGraw-Hill, New York, 1953.

DOCUMENT CONTROL DATA - R & D

(Security classification of title, body of abstract and indexing annotation must be entered when the overall report is classified)

1. ORIGINATING ACTIVITY (Corporate author)	2a. REPORT SECURITY CLASSIFICATION
Whittaker Corporation Research & Development/San Diego San Diego, California	Unclassified
	2b. GROUP

3. REPORT TITLE

APPLICATION OF MICROMECHANICS TO JOINTS AND CUTOUTS

4. DESCRIPTIVE NOTES (Type of report and inclusive dates)

Final Technical Report

5. AUTHOR(S) (First name, middle initial, last name)

Alberto H. Puppo
Dr. Juan A. Haener

6. REPORT DATE	7a. TOTAL NO. OF PAGES	7b. NO. OF REFS
April 1969	78	16

8a. CONTRACT OR GRANT NO. DAAJ02-67-0093	9a. ORIGINATOR'S REPORT NUMBER(S)
b. PROJECT NO. Task 1F162204A17002	USAAVLABS Technical Report 69-25
c.	9b. OTHER REPORT NO(S) (Any other numbers that may be assigned this report)
d.	Whittaker MJO 323 Final Report

10. DISTRIBUTION STATEMENT

This document has been approved for public release and sale; its distribution is unlimited.

11. SUPPLEMENTARY NOTES	12. SPONSORING MILITARY ACTIVITY
	U.S. Army Aviation Materiel Laboratories Fort Eustis, Virginia

13. ABSTRACT

In this report the stress distribution in loop and bolt joints made of composite materials is studied using analytical and experimental methods. Also, the stress concentration in orthotropic composite sheets with a circular hole is studied.

The numerical technique to evaluate the stresses and displacements is described. Simple design formulas to compute the stresses at critical regions are developed. A procedure of structural design is delineated and applied to specific cases.

Experimental results obtained by testing composite joints are reported. Stress distribution tests were performed using the photoelastic technique. Failure location and ultimate loads for several composite joints are shown.

This report contains the analysis of the stress concentration that appears around a circular hole in an orthotropic composite sheet under simple tension and simple shear loadings.

DD FORM 1473 REPLACES DD FORM 1473, 1 JAN 64, WHICH IS OBSOLETE FOR ARMY USE.

14. KEY WORDS	LINK A		LINK B		LINK C	
	ROLE	WT	ROLE	WT	ROLE	WT
Micromechanics						
Composite Materials						
Joints of Composite Materials						
Cutouts						